Experiments with Impulsive Motion of a Foil to Generate Large Lift and Thrust Forces

MASSACHUSETTS INSTITUTE OF TECHNOLOGY
SEP 19 2019
LIBRARIES
ARCHIVES

by

Miranda Kotidis

Submitted to the Department of Mechanical Engineering
in partial fulfillment of the requirements for the degree of

Master of Science in Mechanical Engineering

at the

MASSACHUSETTS INSTITUTE OF TECHNOLOGY

September 2019

© Massachusetts Institute of Technology 2019. All rights reserved.

Author .... Signature redacted .....
Department of Mechanical Engineering
August 19,2019

Certified by..... Signature redacted ..
Michael Triantafyllou
Professor of Mechanical and Ocean Engineering
Thesis Supervisor

Accepted by ..... Signature redacted
Nicolas Hadjiconstantinou
Chair, Mechanical Engineering Granduate Program Committee

Experiments with Impulsive Motion of a Foil to Generate Large Lift and Thrust Forces

by

Miranda Kotidis

Submitted to the Department of Mechanical Engineering
on August 19,2019, in partial fulfillment of the
requirements for the degree of
Master of Science in Mechanical Engineering

Abstract

As underwater vehicles become increasingly versatile and capable, bio-inspired propulsion systems are becoming a viable possibility for future vehicles. In particular, flapping foil actuators are promising in their abilities for propulsion and maneuvering. Current underwater vehicles rely on propellers, which form a jet wake to produce propulsion forces, and, as such, experience an inherent delay between the movement of the propeller and the vehicle feeling a propulsive force. To mitigate this shortcoming, flapping foils were moved in swift, one-time strokes to produce large, transient forces in still water to produce propulsive and/or maneuvering forces almost instantaneously. Previous work produced trajectories, characterized by heave and pitch motions, for which the lift and thrust profiles were confirmed. These strokes take advantage of added mass/inertial effects to produce propulsive forces useful for maintaining position or orientation or for precise maneuverability. Various novel combinations of heave and pitch motions were tested and dye visualization was performed with a custom wing to elucidate the wake and vortical structures produced by these strokes.

Thesis Supervisor: Michael Triantafyllou
Title: Professor of Mechanical and Ocean Engineering

Acknowledgments

First of all, thank you to Prof. Michael Triantafyllou, for his guidance and advice during my graduate research so far. I would also like to thank my all my labmates and fellow Tow Tank students, past and present, for all their support and problem-solving help. Last, but certainly not least, thank you to all my colleages and friends in the MIT community, my family, and Drew for all their support, love, and friendship. I could not have done it without all of you.

Contents

1 Introduction **13**

1.1 Motivation 13

1.2 Background 14

1.2.1 Previous work 14

1.2.2 Verification experiments 16

2 Experimental Setup **23**

2.1 Kinematics and Force Definintions 23

2.2 Experimental Apparatus Setup 24

2.3 Dye Visualization Setup 24

3 Experiments and Results **29**

3.1 Trajectory 1.1 29

3.1.1 Kinematics 29

3.1.2 Force Results 30

3.1.3 Dye Visualisation 32

3.2 Trajectory 4 32

3.2.1 Kinematics 32

3.2.2 Force Results 33

3.2.3 Dye Visualisation 34

3.3 Trajectory 5 37

3.3.1 Kinematics 37

3.3.2 Force Results 37

3.3.3 Dye Visualisation 38
3.4 Trajectory 6.1 40
3.4.1 Kinematics 40
3.4.2 Force Results 40
3.4.3 Dye Visualisation 41
3.5 Trajectory 6.2 44
3.5.1 Kinematics 44
3.5.2 Force Results 45
3.6 Trajectory 6.3 47
3.6.1 Kinematics 47
3.6.2 Force Results 49
3.6.3 Dye Visualisation 50

4 Conclusion **53**

A Dye Visualization Speed Comparison **55**

List of Figures

1-1 Method I kinematics, taken with permission from (Triantafyllou et al., 2003) 15

1-2 Method I force results, taken with permission from (Triantafyllou et al., 2003) 15

1-3 Method II kinematics, taken with permission from (Triantafyllou et al., 2003) 16

1-4 Method II force results, taken with permission from (Triantafyllou et al., 2003). These results were compared to the force results in Section 1.2.2. 16

1-5 Kinematics of the foil's motion during Trajectory 1. Heave and pitch position are shown in (a), heave and pitch velocity are shown in (b), and heave and pitch acceleration are shown in (c). 17

1-6 Visualization of the foil's motion during Trajectory 1. 17

1-7 Force results from Trajectory 1. Presented here as C_L and C_T, as described in Section 2.1 18

1-8 Method I force results (top), taken with permission from (Triantafyllou et al., 2003), and a resized Trajectory 1 results, same as in Figure 1-7. There are obvious similarities in the force profiles, but for quantitative comparison, (Triantafyllou et al., 2003) found the peak lift coefficient to be around 8 and the peak thrust coefficient to be around -2, with which the current results agree. 19

1-9 Kinematics of the foil's motion during Trajectory 2. Heave and pitch position are shown in (a), heave and pitch velocity are shown in (b), and heave and pitch acceleration are shown in (c). 20

1-10 Visualization of the foil's motion during Trajectory 2. 20

1-11 Force results from Trajectory 2. Presented here as C_L and C_T, as described in Section 2.1 21

1-12 Method II force results (top), taken with permission from (Triantafyllou et al., 2003), and a resized version of the Trajectory 2 results, same as in Figure 1-11. There are obvious similarities in the force profiles, but for quantitative comparison, (Triantafyllou et al., 2003) found the peak lift coefficient to be around 9 and the peak thrust coefficient to be around 6, with which the current results agree. 21

2-1 (a) MIT Testing Tank. The actuators move the foil according to the specified trajectory and the resulting forces are recorded by the Forcemeter and imported to MATLAB for post processing. (b) Foil Dimensions. These values of span and chord are used to calculate the Lift and Thrust coefficients as shown in Equation 2.1 24

2-2 Kinematics of the foil's motion and resulting force convention. The foil moves in heave and pitch through the prescreibed trajectory, and the forces are recorded 25

2-3 SolidWorks CAD model of the custom wing designed for dye visualization. The full, solid model is shown in (a), and a transparent version showing the interior channels is shown in (b). The six injection points are at the leading and trailing edges of the cross section at three points along the span of the wing. The middle two points were used during the experiments. 26

2-4 Fabricated wing for dye visualization. The wing pieces were printed on a Form II printer, assembled and sanded, and sprayed with waterproof paint to be visible underwater. 27

2-5 Testing Tank outfitted with lights and cameras to record wake videos. 28

3-1 Kinematics of the foil's motion during Trajectory 1.1. Heave and pitch position are shown in (a), heave and pitch velocity are shown in (b), and heave and pitch acceleration are shown in (c). 29

3-2 Visualization of the foil's motion during Trajectory 1.1. 30

3-3 Force results from Trajectory 1.1. Presented here as C_L and C_T, as described in Section 2.1 31

3-4 Visualization of the forces produced by Trajectory 1.1. The foil outlines and red arrows representing the forces are scaled for visual purposes. 31

3-5 Dye visualization images and diagram from Trajectory 1.1. 33

3-6 Kinematics of the foil's motion during Trajectory 4. Heave and pitch position are shown in (a), heave and pitch velocity are shown in (b), and heave and pitch acceleration are shown in (c). 34

3-7 Visualization of the foil's motion during Trajectory 4. 34

3-8 Force results from Trajectory 4. Presented here as C_L and C_T, as described in Section 2.1 35

3-9 Visualization of the forces produced by Trajectory 4. 35

3-10 Dye visualization images and diagram of Trajectory 4. 36

3-11 Kinematics of the foil's motion during Trajectory 5. Heave and pitch position are shown in (a), heave and pitch velocity are shown in (b), and heave and pitch acceleration are shown in (c). 37

3-12 Visualization of the foil's motion during Trajectory 5. 38

3-13 Force results from Trajectory 5. Presented here as C_L and C_T, as described in Section 2.1 39

3-14 Visualization of the forces produced by Trajectory 5. 39

3-15 Dye visualization images and diagram of Trajectory 5. 41

3-16 Kinematics of the foil's motion during Trajectory 6.1. Heave and pitch position are shown in (a), heave and pitch velocity are shown in (b), and heave and pitch acceleration are shown in (c). 42

3-17 Visualization of the foil's motion during Trajectory 6.1. 42
3-18 Force results from Trajectory 6.1. Presented here as C_L and C_T, as described in Section 2.1 43
3-19 Visualization of the forces produced by Trajectory 6.1. 43
3-20 Dye visualization images from Trajectory 6.1. 44
3-21 Kinematics of the foil's motion during Trajectory 6.2. Heave and pitch position are shown in (a), heave and pitch velocity are shown in (b), and heave and pitch acceleration are shown in (c). 45
3-22 Visualization of the foil's motion during Trajectory 6.2. 45
3-23 Force results from Trajectory 6.2. Presented here as C_L and C_T, as described in Section 2.1 46
3-24 Visualization of the forces produced by Trajectory 6.2. 46
3-25 Dye visualization images from Trajectory 6.2. 48
3-26 Kinematics of the foil's motion during Trajectory 6.3. Heave and pitch positions are shown in (a), heave and pitch velocities are shown in (b), and heave and pitch accelerations are shown in (c). 49
3-27 Visualization of the foil's motion during Trajectory 6.3. 49
3-28 Force results from Trajectory 6.3 Presented here as C_L and C_T, as described in Section 2.1 50
3-29 Visualization of the forces produced by Trajectory 6.3. 50
3-30 Dye visualization images from Trajectory 6.3. 52

Chapter 1

Introduction

1.1 Motivation

Underwater vehicles are emerging as incredibly effective platforms for ocean monitoring and exploration, underwater structure installation and maintenance, and accident/hazard mitigation (Triantafyllou, 2017). They have allowed humans to interact with and study otherwise unreachable underwater environments, and their capabilities are broadening as autonomous underwater vehicles are becoming increasingly common. Although plenty of research has been done to improve these vehicles' versatility and functionality, one aspect of their design has remained relatively constant: their propulsion. Underwater vehicles have traditionally relied on rotary thrusters or propellers to generate forces and move the vehicle and/or respond to disturbances in the environment. These types of actuators produce a jet-like wake, which then produces the necessary force to move the vehicle; however, the formation of this wake is not instantaneous, and, as a result, the forces felt by the vehicle are delayed. This inherent delay makes these vehicles very difficult to control, because oftentimes a sharp force is required to intervene and maintain the vehicle's position or direction in an unsteady current or wave, or to counteract forces created by manipulators onboard the vehicle.

In order to minimize or even eliminate this delay, new types of bio-mimetic actuators are being developed. Nature has provided an enormous amount of inspiration,

since almost all underwater animals that swim can change direction almost instantly and can move from a standstill in the blink of an eye. Many fish and cephalopods even remain perfectly balanced as waves and currents go by, or when moving various parts of their bodies (i.e. extending a part of their body to catch prey). More specifically, many fish use their pectoral and pelvic fins to produce the forces necessary to remain balanced and to precisely control their position or direction of movement (Lauder et al., 2007) (Lauder and Madden, 2006) (Lauder et al., 2006). By modeling the fins as flapping hydrofoils, large, transient forces can be produced through combinations of heave and pitch motions.

1.2 Background

Previous experiments have shown that, through relatively simple trajectories in heave and pitch, a flapping hydrofoil can create large forces quite rapidly (Read et al., 2003) (Licht et al., 2004) (Triantafyllou et al., 2003). The work done in (Triantafyllou et al., 2003) served as inspiration and a starting point for the current experiments.

1.2.1 Previous work

In (Triantafyllou et al., 2003), the experiments showed the promising nature of flapping foils with no incoming velocity, i.e. in calm water. The foil followed simulataneous partial cycles of sinusoidial heave and pitch motions for rapid development of forces.

Method I

The first swift motion tested in (Triantafyllou et al., 2003) was referred to as Method I. This method began with the foil horizontal in the $\theta = 0$ position, and sweeps to $\theta = +\pi/2$ as it moves downward in heave. Figure 1-1 shows the foil's movement. The force results are shown in Figure 1-2 and feature a large lift force coupled with very small (if any) thrust force. Even though the units in Figure 1-2 are Newtons, the peak lift coefficient was around 6, and the peak thrust coefficient was around -2 from

(Triantafyllou et al., 2003). This experiment was recreated and discussed in Section 1.2.2.

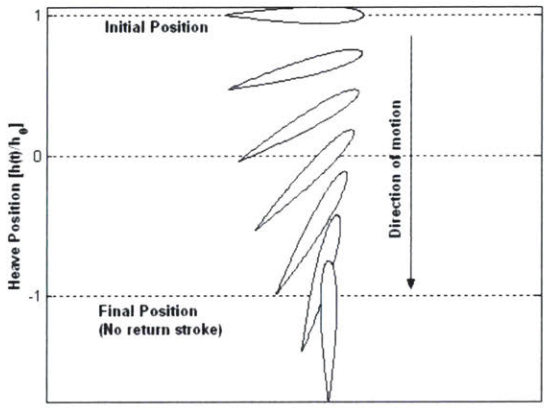

Figure 1-1: Method I kinematics, taken with permission from (Triantafyllou et al., 2003)

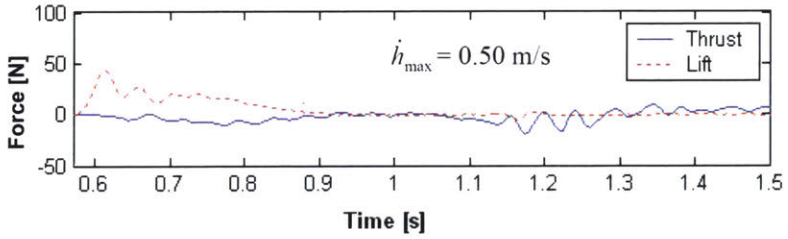

Figure 1-2: Method I force results, taken with permission from (Triantafyllou et al., 2003)

Method II

The second swift motion tested was referred to in (Triantafyllou et al., 2003) as Method II. This method began with the foil vertical in the $\theta = -\pi/2$ position, and sweeps to $\theta = +\pi/2$ as it moves downward in heave. Figure 1-3 shows the foil's movement. The force results are shown in Figure 1-4 and feature a large lift force coupled with very small (if any) thrust force. Even though the units in Figure 1-4 were Newtons, the peak lift coefficient was around 9, and the peak thrust coefficient was around 6 (Triantafyllou et al., 2003). This experiment was recreated and discussed in Section 1.2.2.

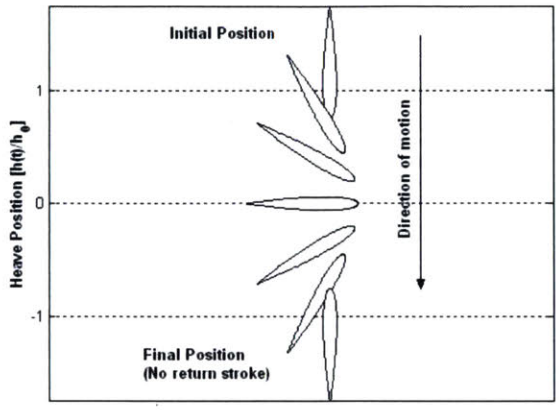

Figure 1-3: Method II kinematics, taken with permission from (Triantafyllou et al., 2003)

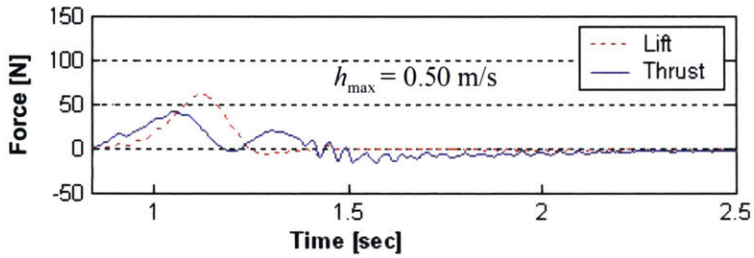

Figure 1-4: Method II force results, taken with permission from (Triantafyllou et al., 2003). These results were compared to the force results in Section 1.2.2.

1.2.2 Verification experiments

As discussed in Section 1.2.1, the two methods found in previous experiments were recreated using the experimental setup in the MIT Testing Tank, described in Section 2.

Trajectory 1

Trajectory 1 is a recreation of Method I from (Triantafyllou et al., 2003), and introduced in Section 1.2.1. Just like Method I, Trajectory 1 begins with the foil horizontal at the $\theta = 0$ position, and sweeps to the $\theta = +\pi/2$ as it moves downward in heave. Figure 1-5 shows the kinematics of this trajectory. Figure 1-5(a) shows the heave and pitch positions over time, (b) shows the heave and pitch velocities, and (c) shows the heave and pitch accelerations. Both the heave and pitch follow partial sinusoids, and

are smooth. Figure 1-6 shows a visualization of the foil's trajectory.

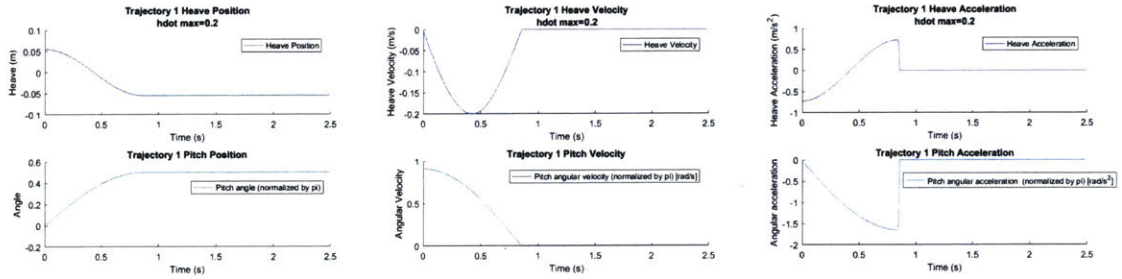

(a) (b) (c)

Figure 1-5: Kinematics of the foil's motion during Trajectory 1. Heave and pitch position are shown in (a), heave and pitch velocity are shown in (b), and heave and pitch acceleration are shown in (c).

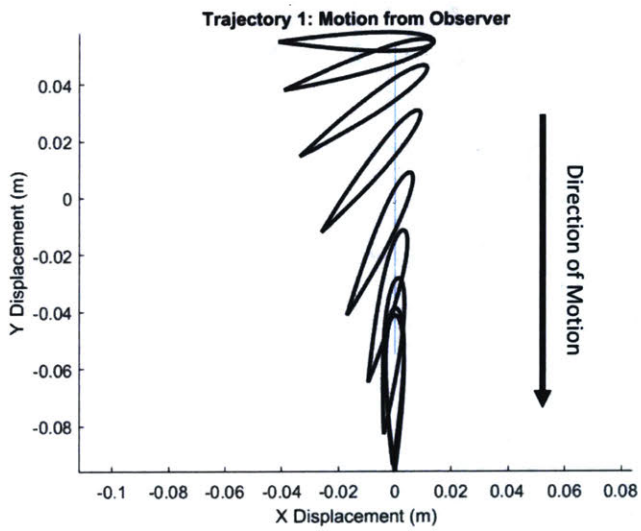

Figure 1-6: Visualization of the foil's motion during Trajectory 1.

The force results for Trajectory 1 are presented in Figure 1-7, presented in the non-dimensional form described in Section 2.1 and Equation 2.1. A large lift force peak accompanied by a small negative peak in thrust appears in both sets of results.

To compare Trajecotry 1 to Method I from the previous work, Figure 1-8 shows the results from both (Triantafyllou et al., 2003) (top) and a resized version of Figure 1-7 (bottom), showing clear similarities in the force profiles. Both sets of results show a large lift force with a small, negative thrust force. For quantitative comparisons, we use the peak lift/thrust coefficients. As mentioned in Section 1.2.1, (Triantafyllou

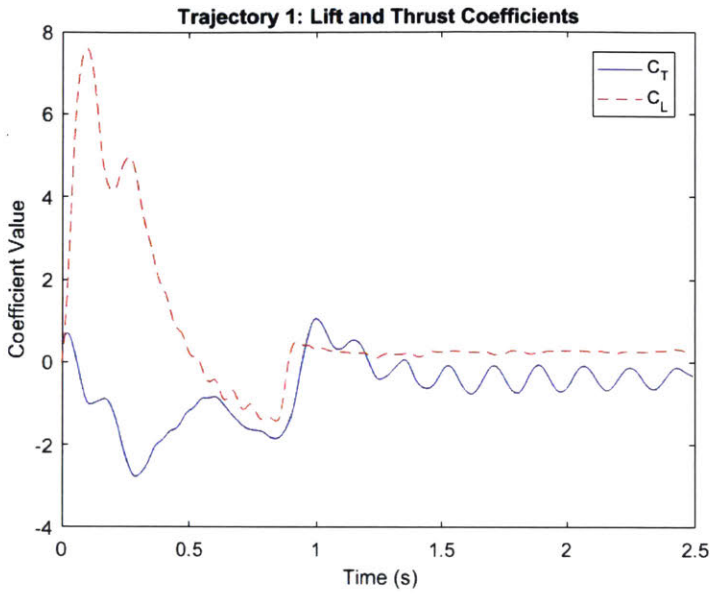

Figure 1-7: Force results from Trajectory 1. Presented here as C_L and C_T, as described in Section 2.1

et al., 2003) found a peak lift coefficient of around 8 and a peak thrust coefficient of -2. These results match very well to the peaks in the current experiments, which also had a peak lift coefficient of around 8, and a peak thrust coefficient of around -2.5. Therefore, the current experiments match the previous work.

Trajectory 2

Trajectory 2 is a recreation of Method II from (Triantafyllou et al., 2003), and introduced in Section 1.2.1. Just like Method II, Trajectory 2 begins with the foil vertical at the $\theta = +\pi/2$ position, and sweeps to the $\theta = +\pi/2$ as it moves downward in heave. Figure 1-9 shows the kinematics of this trajectory. Figure 1-9(a) shows the heave and pitch positions over time, (b) shows the heave and pitch velocities, and (c) shows the heave and pitch accelerations. Both the heave and pitch follow partial sinusoids, and are smooth. Figure 1-10 shows a visualization of the foil's trajectory.

The force results for Trajectory 2 are presented in Figure 1-11, presented in non-dimensional form described in Section 2.1 and Equation 2.1. Here, the trajectory produces a large positive lift force accompanied by two smaller but positive thrust forces.

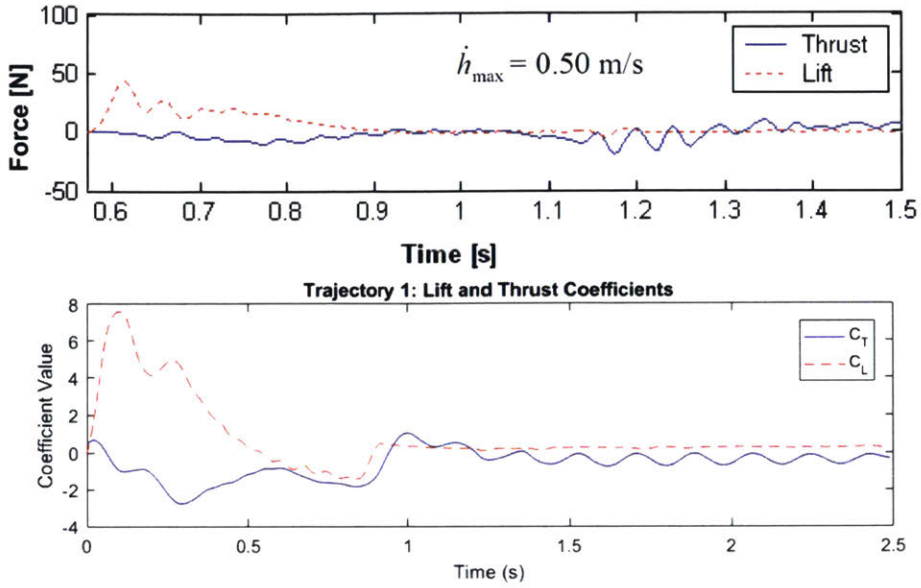

Figure 1-8: Method I force results (top), taken with permission from (Triantafyllou et al., 2003), and a resized Trajectory 1 results, same as in Figure 1-7. There are obvious similarities in the force profiles, but for quantitative comparison, (Triantafyllou et al., 2003) found the peak lift coefficient to be around 8 and the peak thrust coefficient to be around -2, with which the current results agree.

To compare Trajecotry 2 to Method II from the previous work, Figure 1-12 shows the results from both (Triantafyllou et al., 2003) (top) and a resized version of Figure 1-11 (bottom), showing clear similarities in the force profiles. Both sets of results show a large lift force with two smaller thrust peaks, one just before the lift peak, and one just after. For quantitative comparisons, we use the peak lift/thrust coefficients. As mentioned in Section 1.2.1, (Triantafyllou et al., 2003) found a peak lift coefficient of around 9 and a peak thrust coefficient of 6. These results match very well to the peaks in the current experiments, which also had a peak lift coefficient of around 10, and a peak thrust coefficient of around 6. Therefore, the current experiments match the previous work.

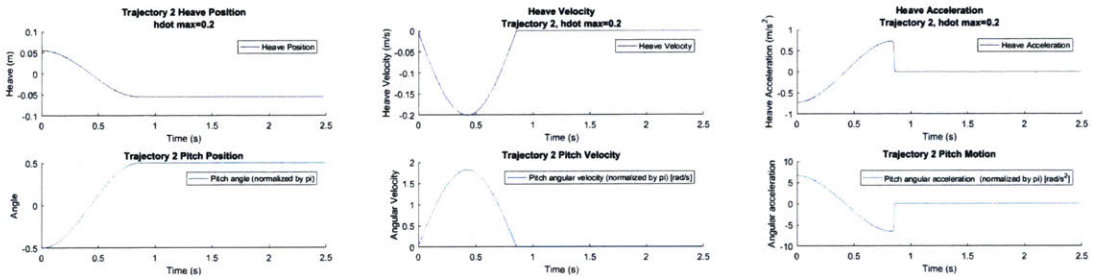

(a) (b) (c)

Figure 1-9: Kinematics of the foil's motion during Trajectory 2. Heave and pitch position are shown in (a), heave and pitch velocity are shown in (b), and heave and pitch acceleration are shown in (c).

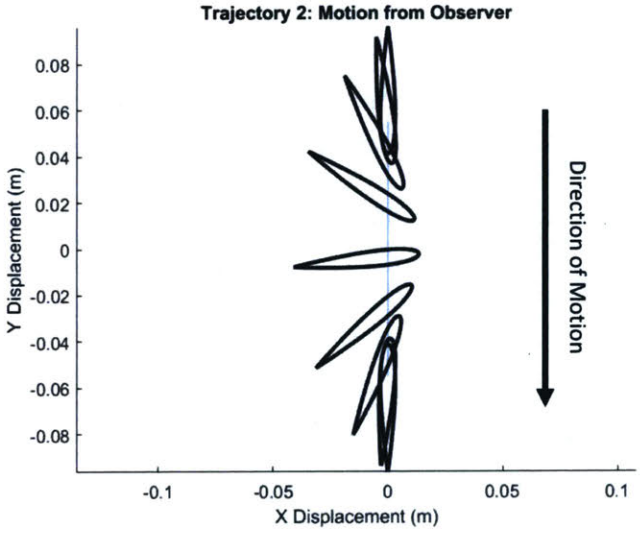

Figure 1-10: Visualization of the foil's motion during Trajectory 2.

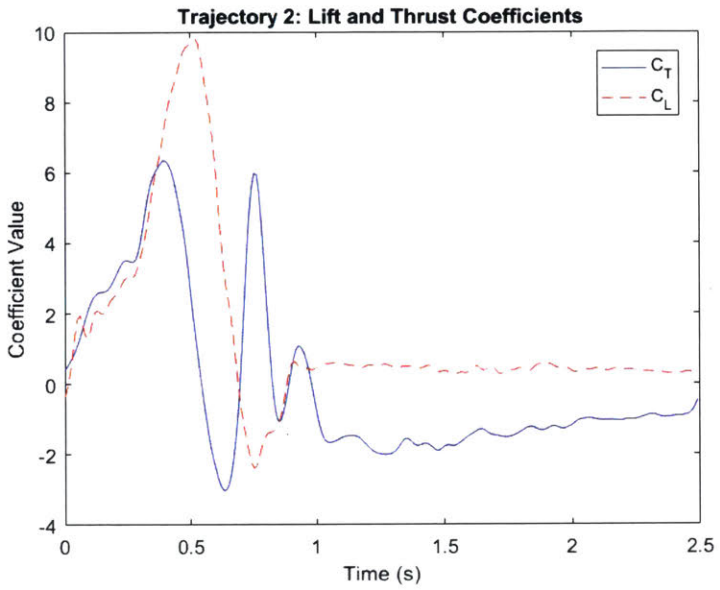

Figure 1-11: Force results from Trajectory 2. Presented here as C_L and C_T, as described in Section 2.1

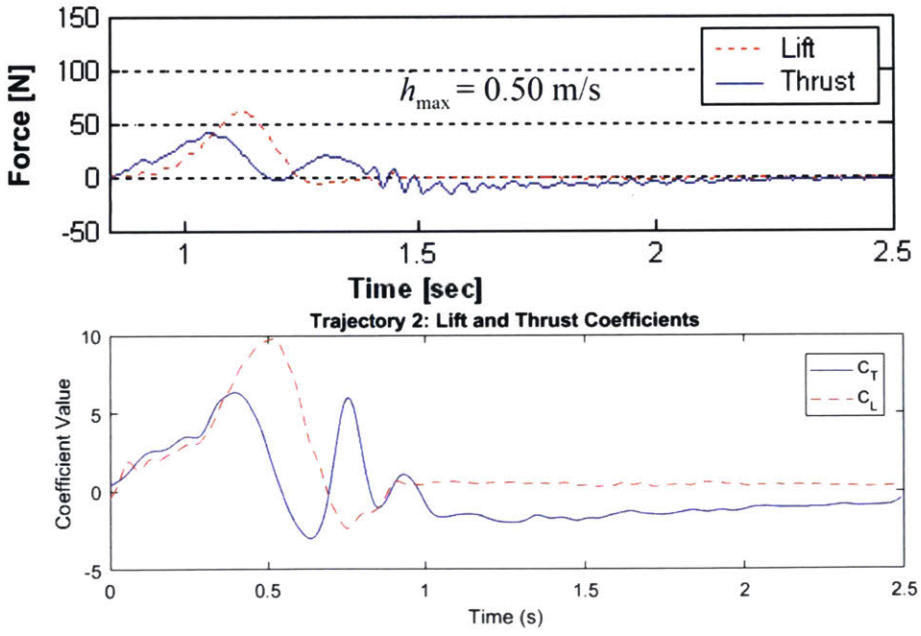

Figure 1-12: Method II force results (top), taken with permission from (Triantafyllou et al., 2003), and a resized version of the Trajectory 2 results, same as in Figure 1-11. There are obvious similarities in the force profiles, but for quantitative comparison, (Triantafyllou et al., 2003) found the peak lift coefficient to be around 9 and the peak thrust coefficient to be around 6, with which the current results agree.

Chapter 2

Experimental Setup

2.1 Kinematics and Force Definintions

In (Triantafyllou et al., 2003), the trajectories were fully defined by a heave function $h(t)$ and a pitch function $\theta(t)$. These definitions were continued in this work; $h(t)$ controls the vertical motion of the trajectory, while $\theta(t)$ controls the angle of the foil in radians, with respect to horizontal. In the experiments, the heave and often the pitch followed a fraction of a sinusoid, which ensured smooth movements through the water, and the speed of the trajectory is controlled by the maximum heave velocity, $\dot{h}_{max}$ (in m/s). The forces produced by the foil were measured as global vertical and horizontal forces, known as lift (positive y-direction force) and thrust (postivie x-direction force). Lift and thrust coefficients were calculated using Equation 2.1, below, where ρ is the density of water ($\rho = 1000\ kg/m^3$ in these experiments), c is the chord length of the foil, and s is the span of the foil.

$$C_{lift,thrust} = \frac{F_{lift,thrust}}{\frac{1}{2}\rho \dot{h}_{max}^2 cs} \tag{2.1}$$

2.2 Experimental Apparatus Setup

Experiments were done in the MIT Testing Tank. Figure 2-1(a) shows the Testing Tank, and Figure 2-1(b) shows the NACA 0012 foil used in the force experiments, with a span on $s = 0.36m$ (14.17 in) and chord $c = 0.055m$ (2.16 in). In the experiments, the foil moves in combinations of heave and pitch (around the quarter-chord, and the resulting force data was recorded using an ATI Gamma force sensor (Model No: 12345) and was imported for post processing and calculations of the Lift and Thrust Coefficients. Figure 2-2 shows the conventions for the kinematics and dynamics of the foil used throughout these experiments. For consistency, force coefficients calculated in Equation 2.1 correlate to the C_L and C_T in the figure.

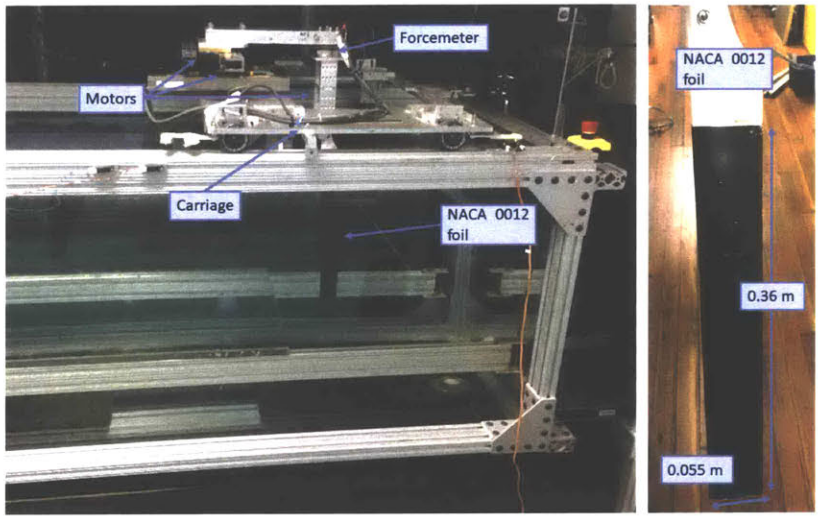

(a) (b)

Figure 2-1: (a) MIT Testing Tank. The actuators move the foil according to the specified trajectory and the resulting forces are recorded by the Forcemeter and imported to MATLAB for post processing. (b) Foil Dimensions. These values of span and chord are used to calculate the Lift and Thrust coefficients as shown in Equation 2.1

2.3 Dye Visualization Setup

In addition to the force measurements, dye visualization experiments helped to elucidate the wake produced by these swift motions in heave and pitch. In order to inject

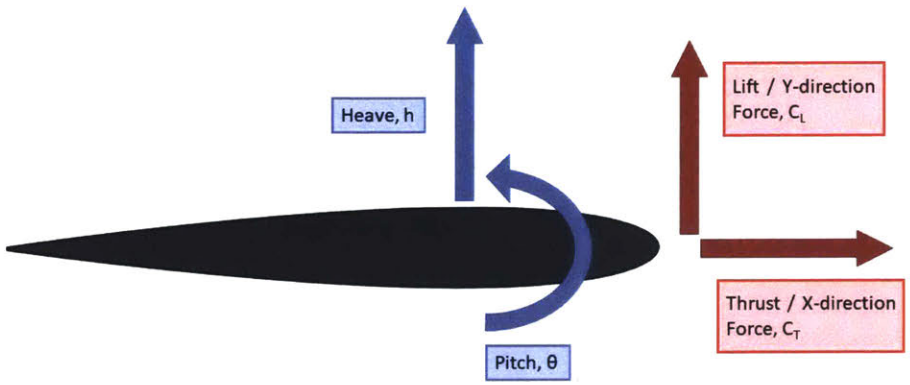

Figure 2-2: Kinematics of the foil's motion and resulting force convention. The foil moves in heave and pitch through the prescreibed trajectory, and the forces are recorded

dye into the flow without disturbing it, a custom wing was designed with interiror channels for the dye to flow through. The dye was originally planned to be injected into the flow at six locations, at the leading and traling edge of the wing at three different locations along the span; however, only two injection points ended up being used - one at the leading edge and one at the trailing edge approximately halfway down the span.

Figure 2-3 shows the Solidworks model of the entire foil. Holes at the top of the wing allow the dye tubing system to be removeable for motor calibration and initialization without tangling. The top section of the wing was designed to integrate seamlessly into the existing bracket seen in Figure 2-1(b) used to attach the foil to the motor assembly. The foil cross section has the same profile as the wing used for the force experiments, mentioned in Section 2.2, a NACA 0012 foil with a span of s = 0.36 m (14.17 in) and chord of c = 0.055 m (2.16 in). For fabrication, the wing was divided into four sections for 3D printing. The pieces were printed on a Form II printer in Clear Resin (FormLabs, 2018), and then pieced together with epoxy, sanded smooth, and then sprayed with waterproof paint to be able to be seen by the camera underwater. The actual wing is shown in Figure 2-4.

In order to record the wake, GoPro cameras was mounted to the Testing Tank carriage and lights were mounted to a frame that was placed in the Testing Tank.

Figure 2.3 shows the setup for recording wake videos. As shown by the coordinate axes in the figure, Camera A was located in the positive Y Direction, and Camera B was located in the negative Y direction. Using both cameras allowed the wake structures to be viewed from multiple angles, and captured wake structures both in the beginnings and ends of the trajectories. Red dye was set up to flow from the leading edge, and blue dye flowed from the trailing edge, and the tubes seen in the figure connect the wing's internal channels to the holding containers. As the foil moves through the specified trajectory, the dyes flow through the channels and then the holes in the wing and the cameras capture the wake. The videos recorded by the cameras were then imported and analyzed. For some of the trajectories, only one camera's view was needed to elucidate the wake, while for others both views were used to fully understand the wake structures.

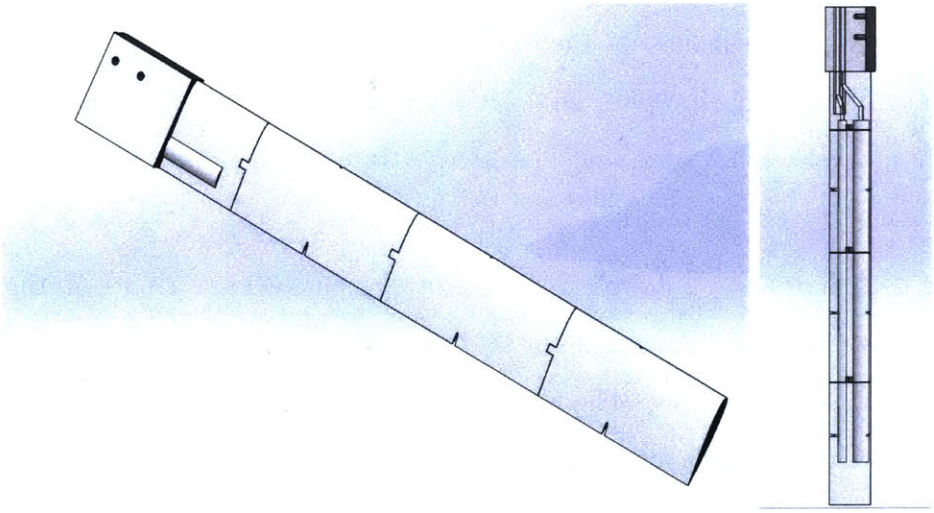

(a) (b)

Figure 2-3: SolidWorks CAD model of the custom wing designed for dye visualization. The full, solid model is shown in (a), and a transparent version showing the interior channels is shown in (b). The six injection points are at the leading and trailing edges of the cross section at three points along the span of the wing. The middle two points were used during the experiments.

Figure 2-4: Fabricated wing for dye visualization. The wing pieces were printed on a Form II printer, assembled and sanded, and sprayed with waterproof paint to be visible underwater.

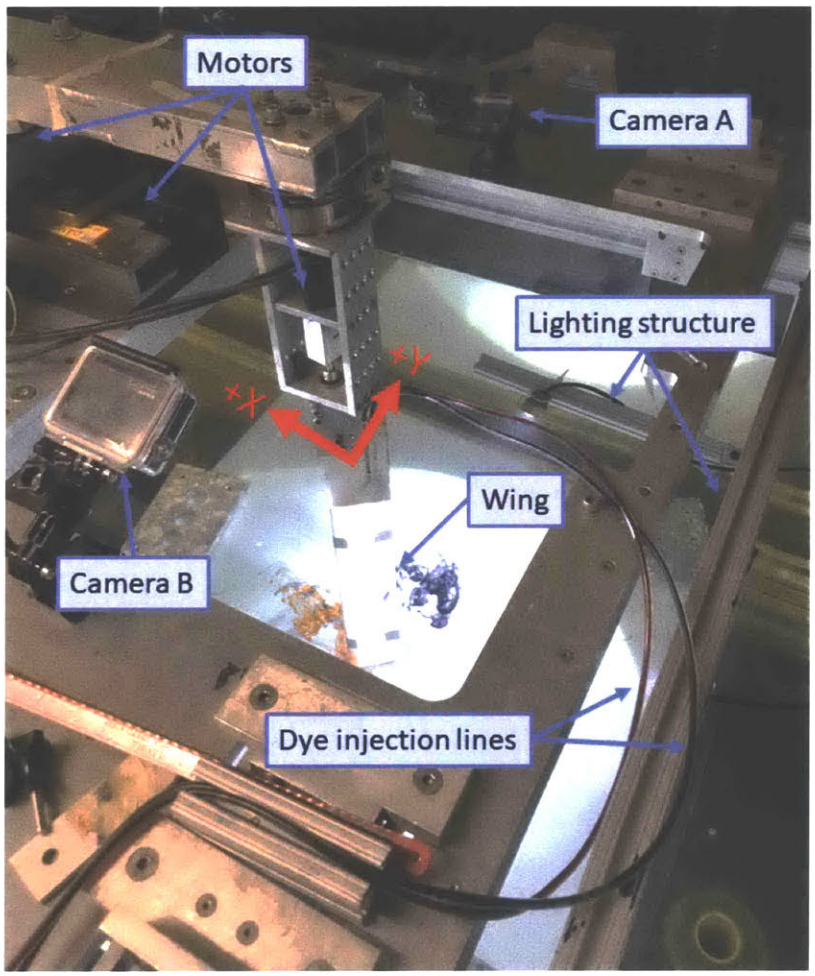

Figure 2-5: Testing Tank outfitted with lights and cameras to record wake videos.

Chapter 3

Experiments and Results

3.1 Trajectory 1.1

3.1.1 Kinematics

This trajectory was directly inspired by Trajectory 1 in Section 1.2.2. Similar to Trajectory 1, Trajectory 1.1 has the foil heaving and pitching simulataneously following partial sinusoids. Trajectory 1.1 differs in that it sweeps from $\theta = 0$ to $\theta = -\pi/2$, pointing downward at the end of the stroke. Figure 3-1 shows a more detailed plot of the foil's heave and pitch motions during Trajectory 1.1, and Figure 3-2 shows a visualization of the foil's movement during Trajectory 1.1.

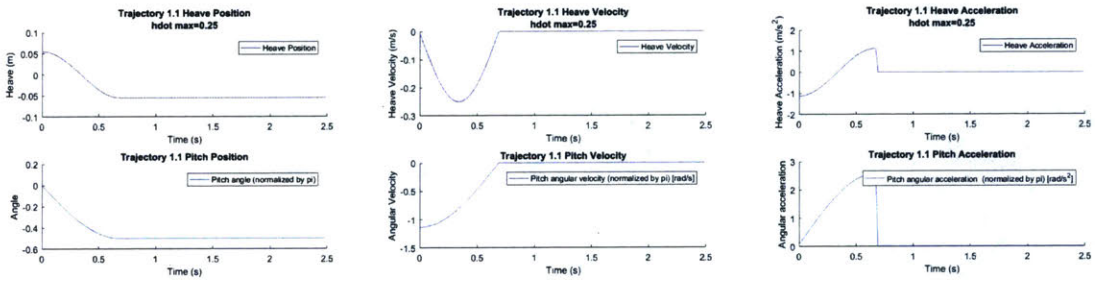

(a) (b) (c)

Figure 3-1: Kinematics of the foil's motion during Trajectory 1.1. Heave and pitch position are shown in (a), heave and pitch velocity are shown in (b), and heave and pitch acceleration are shown in (c).

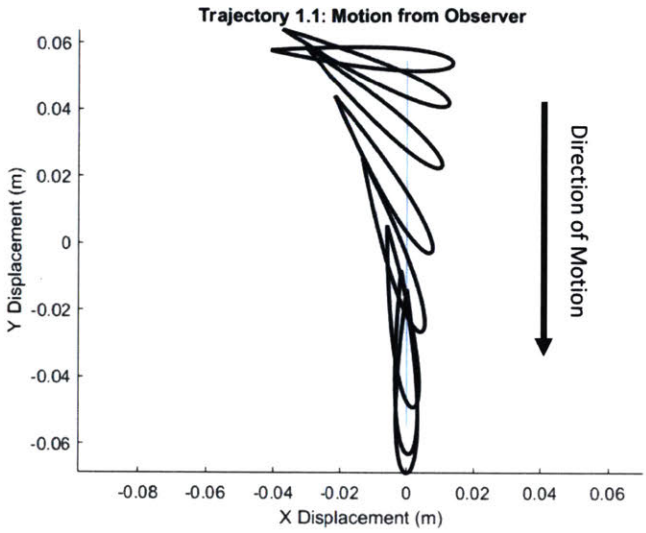

Figure 3-2: Visualization of the foil's motion during Trajectory 1.1.

3.1.2 Force Results

Figure 3-3 shows the force results for Trajectory 1.1, presented non-dimensionally as C_L and C_T. Similar to Trajectory 1 in Section 1.2.2, a large lift force is produced; however here a positive thrust force is produced, whereas Trajectory 1 produced a negative thrust force. This is a result of the pitching motion in Trajectory 1.1 being opposite that of Trajectory 1. Figure 3-4 shows a more intuitive representation of the force data, in a similar fashion to Figure 3-2. For clarity, the force data corresponding to the portion of the trajectory where the foil is actually moving (from $t = 0s$ to $t = 0.7s$) is represented in this figure by red arrows, where inertial forces would be dominant.

While, on first glance, these force results look incredibly promising, if one looks closely, this trajectory produces an odd looking secondary peak when the foil comes to a stop. The foil's motion stops completely by $t = 0.7s$, as seen in Figure 3-1, and one would expect inertial forces to disappear to zero. In fact, the opposite happens; one can see in Figure 3-3 around $t = 0.7s$ a peak in positive thrust (positive x force) and negative lift (negative y force), followed by a small, more longer lasting force in the opposite direction – negative thrust (negative x force) and positive lift (positive y force) directions just before $t = 1.0s$. Additionally, in Figure 3-4, a few seemingly out

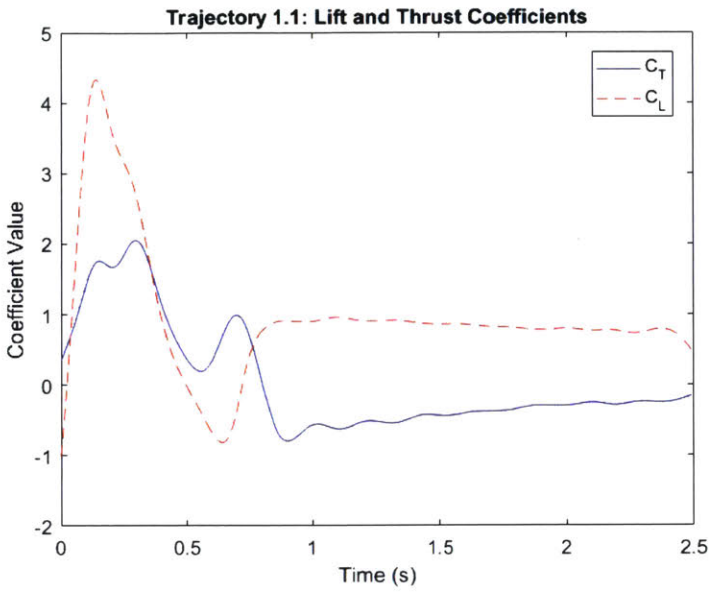

Figure 3-3: Force results from Trajectory 1.1. Presented here as C_L and C_T, as described in Section 2.1

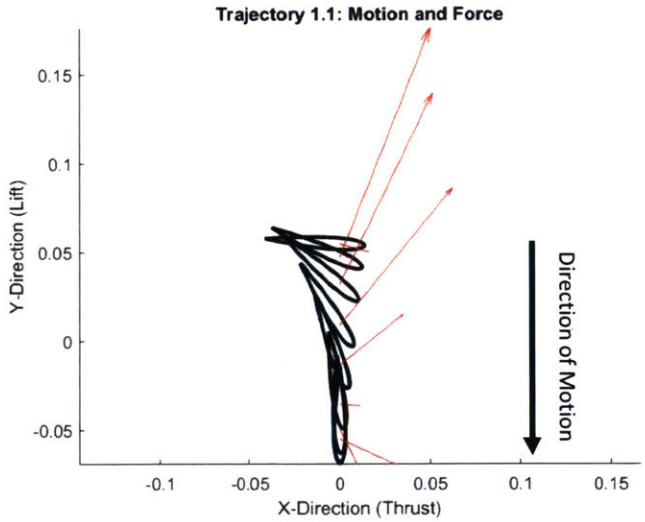

Figure 3-4: Visualization of the forces produced by Trajectory 1.1. The foil outlines and red arrows representing the forces are scaled for visual purposes.

of place vectors appear just as the foil comes to a stop in the positive x and negative y direction. This phenomenon was further investigated through dye visualization experiments using the setup described in Section 2.3, and the results are shown in Figure 3-5.

3.1.3 Dye Visualisation

As explained in Section 2.3, holes in the custom wing allow the dye to flow from the leading and trailing edge, red from the leading edge and blue from the trailing edge. In the beginning of the stroke, the foil produces very obvious leading and trailing edge vortices (LEV in red and TEV in blue), seen in Figure 3-5(a). As the foil continues through the stroke, in Figure 3-5(b)-(c) these vortices move as well; the blue TEV gets left behind as the foil heaves in the negative y direction and does not interact with the TEV at all. The LEV, however, remains very close to the foil throughout the stroke. When the foil stops moving around, as shown in Figure 3-5(d), the LEV is seen right next to the foil's leading edge. It is well-known that vortices produce low-pressure regions, and thus suction forces, and the location of the LEV at this moment would indeed produce a force in the positive x (thrust) and negative y (lift) directions (using the coordinate system on the diagram), exactly what is shown in the force results. Additionally, in Figure 3-5(e), a smaller vortex appears right next to the trailing edge of the foil, which would produce a small force in the negative x (thrust) and positive y (lift) directions – again describing exactly what is shown in the force results.

3.2 Trajectory 4

3.2.1 Kinematics

Trajectory 4 looked into the effect of a asynchronous heave and pitch motion - essentially having heave and pitch move smoothly, but with the pitch motion lasting slightly longer than the heave motion. The foil begins at $\theta = -\pi/4$ and sweeps to $\theta = +\pi/2$, but the frequency of this pitch motion is 3/4 of the frequency of heave, so it finishes the heave motion slightly before the it reaches $\theta = +\pi/2$ position. Figure 3-6 shows a more detailed plot of the foil's heave and pitch motions during Trajectory 4, and Figure 3-7 shows a visualization of the foil's movement during Trajectory 4.

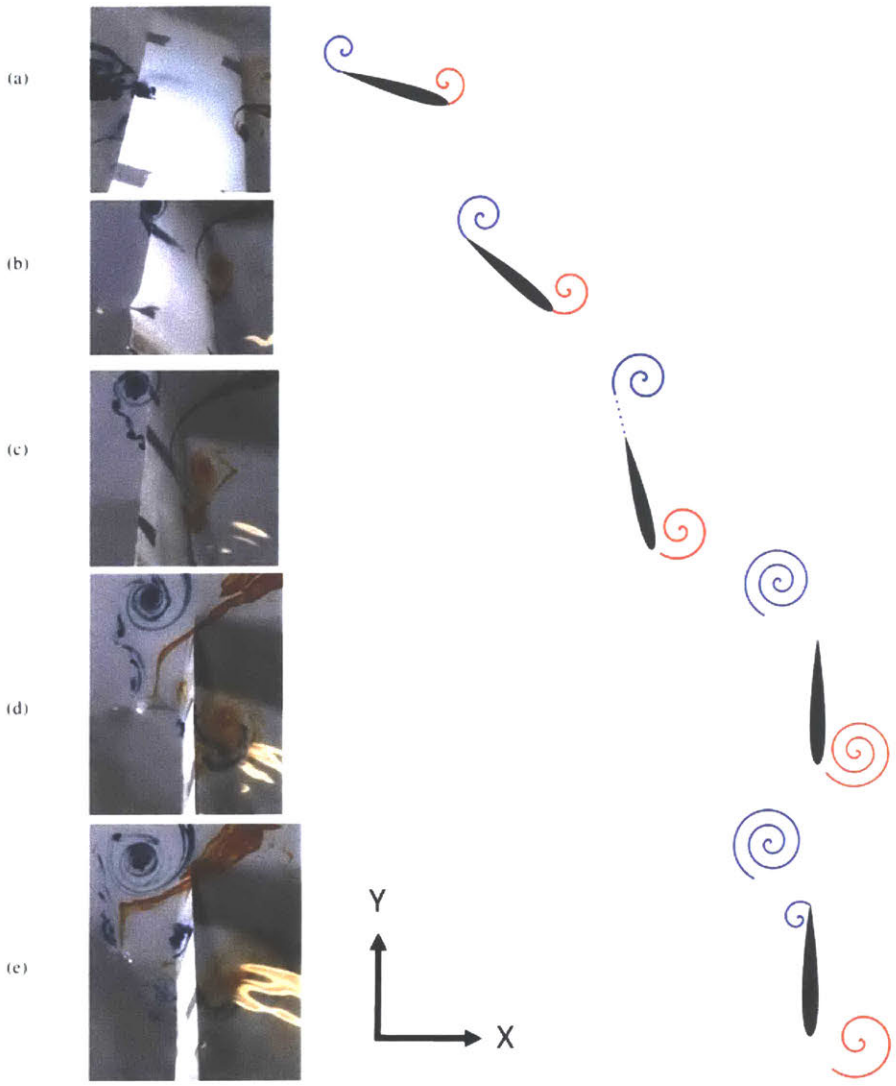

Figure 3-5: Dye visualization images and diagram from Trajectory 1.1.

3.2.2 Force Results

The force data for Trajectory 4 are shown in Figure 3-8, presented in non-dimensional form described in Section 2.1. Additionally, a more intuitive representation of this data is shown in Figure 3-9, and shows the foil's motion with the corresponding force vectors. A large combined peak in both Lift and Thrust forces occurs during the duration of the stroke, with a strange looking secondary peak as the foil comes to a stop. As seen in both Figures 3-8 and 3-9, there is a small peak in a force in the positive X (thrust), negative Y (lift) direction, right as the foil comes to a stop (around 0.5s). This phenomenon was explained using the dye visualization experiments.

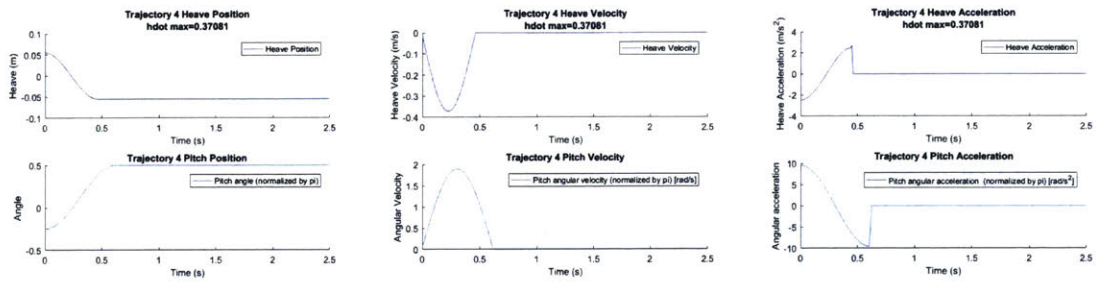

(a) (b) (c)

Figure 3-6: Kinematics of the foil's motion during Trajectory 4. Heave and pitch position are shown in (a), heave and pitch velocity are shown in (b), and heave and pitch acceleration are shown in (c).

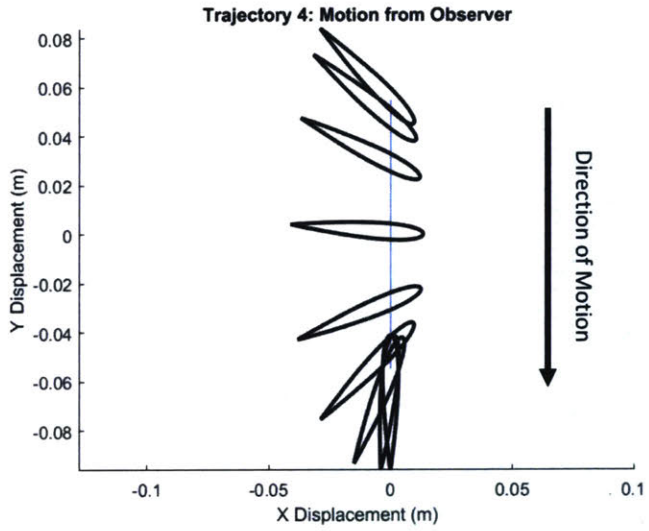

Figure 3-7: Visualization of the foil's motion during Trajectory 4.

3.2.3 Dye Visualisation

For the dye visualization experiment for Trajectory 4, holes in the custom wing allow the dye to flow from the leading and trailing edge, red from the leading edge and blue from the trailing edge. This trajectory was filmed from both cameras as explained in Section 2.3, capturing features from both the beginning and end of the trajectory. Additionally, the dye visualization was performed at a slower speed. This does produce the same flow, as explained in Appendix A. The features from the beginning and middle of the trajectory were best captured by Camera A, and the wake structures at the end of the stroke were best captured by Camera B; however the images have

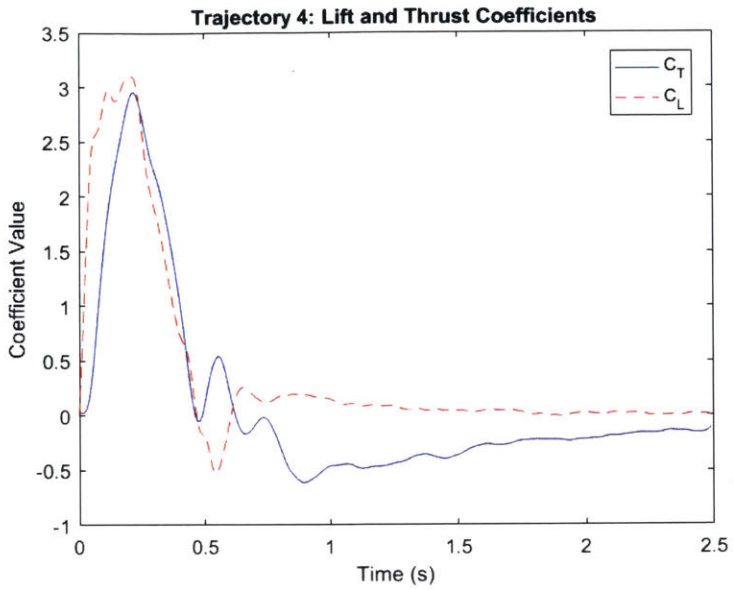

Figure 3-8: Force results from Trajectory 4. Presented here as C_L and C_T, as described in Section 2.1

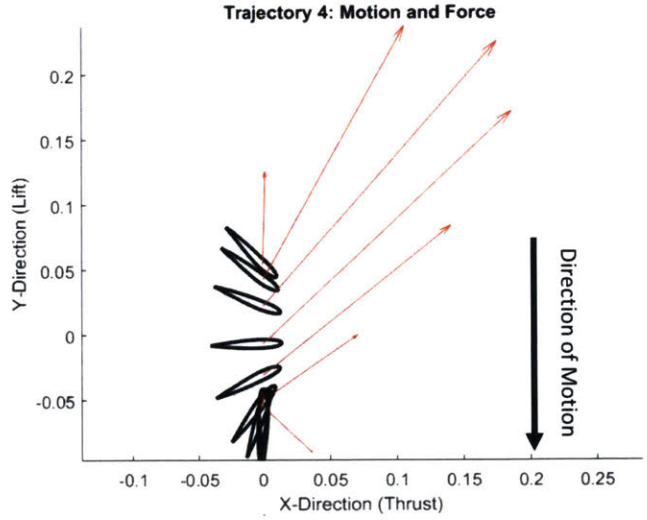

Figure 3-9: Visualization of the forces produced by Trajectory 4.

been rotated/flipped for the diagram.

The wake visualization is presented in Figure 3-10. In Figure 3-10(a), Camera A captured the formation of leading and trailing edge vortices, as the foil begins its motion. Figure 3-10(b) shows the foil with the trailing edge vortex (in blue) detached, but the leading edge vortex (in red) remains attached until the end of the trajectory. In Figure 3-10(c), the foil is beginning its "pure rotation" phase as it rotates without

moving in heave. This causes the red LEV to move into the blue TEV, splitting it up into multiple smaller blue vortices, as seen in Figrure 3-10(d). Additionally, in Figrure 3-10(d), the rotation is complete, and a blue vortex appears just by the trailing edge of the foil. The suction force from this vortex is seen in the smaller peak in the positive X (thrust) and negative Y (lift) direction (following the coordinate system on the figure). The final part of the diagram, Figrure 3-10(e), shows the red LEV pulling some blue dye into it, and pulling the vortex from (d) as well. Since it is so close to the foil, this causes the small force in the negative x (thrust) direction after the foil has stopped moving. Again, we see the "unexplained" forces from the force experiments elucidated as interactions of the foil and the wake structures in the stroke.

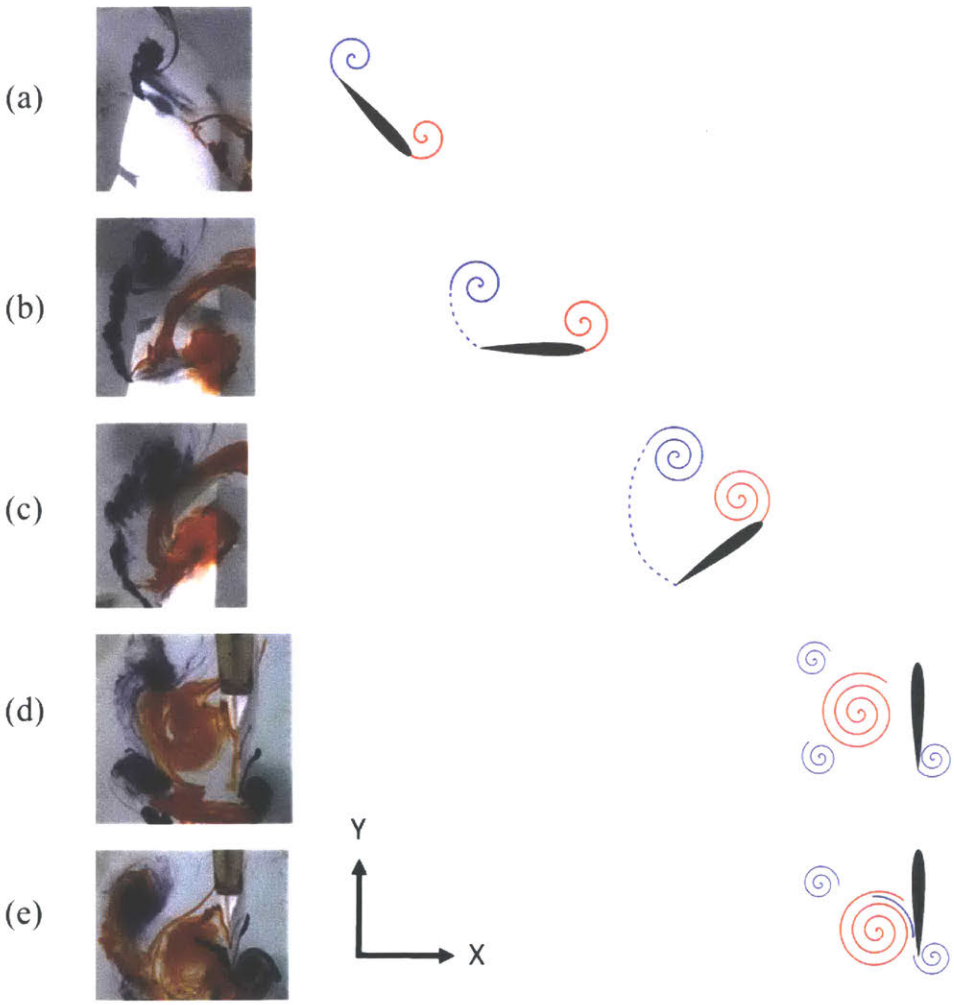

Figure 3-10: Dye visualization images and diagram of Trajectory 4.

3.3 Trajectory 5

3.3.1 Kinematics

This Trajectory was inspired by Trajectory 2 in Section 1.2.2. Starting at $\theta = -3\pi/8$, it sweeps to $\theta = +\pi/4$ and then turns quickly to $\theta = +\pi/2$ by the halfway point of the stroke; the rest of the stroke is spent at the $\theta = +\pi/2$ position. Since it is known that the intertial force relates to the acceleration, to avoid any opposite inertial forces, the foil flips to its final pitch position before the heave acceleration switches from negative to positive. Figure 3-11 shows a more detailed description of the trajectory, including heave and pitch positions, velocities, and accelerations. Figure 3-12 shows a visualization of the trajectory. An interesting aspect of this trajectory is that the foil continues to heave after it has reached its final pitch position; while this should not affect any inertial forces, the foil can still interact with the flow and be affected by the wake.

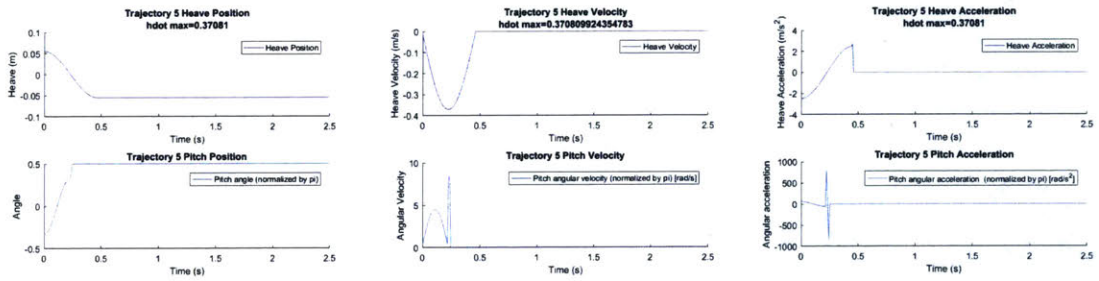

(a) (b) (c)

Figure 3-11: Kinematics of the foil's motion during Trajectory 5. Heave and pitch position are shown in (a), heave and pitch velocity are shown in (b), and heave and pitch acceleration are shown in (c).

3.3.2 Force Results

The force data produced by this trajectory are shown in Figure 3-13, presented in non-dimensional form described in Section 2.1. Here, simultaneous positive peaks of lift and thrust are produced during the motion. The quick-turn maneuver does not seem to affect the force data very much – only a small dip in the lift force is observed.

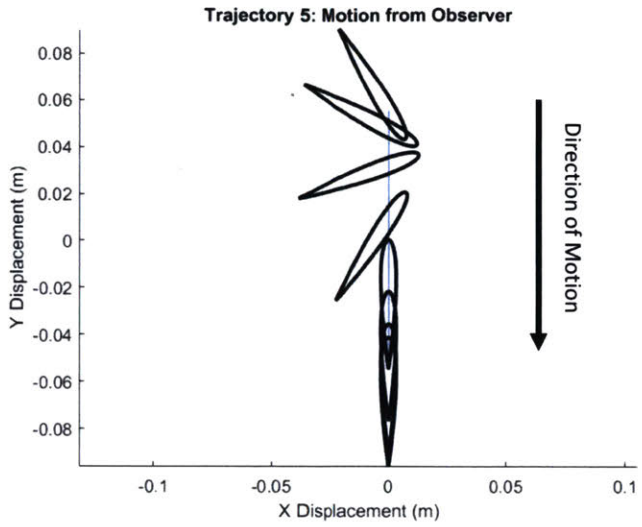

Figure 3-12: Visualization of the foil's motion during Trajectory 5.

A more intuitive representation of this data is shown in Figure 3-14, and shows the foil's motion with the corresponding force vectors. In both representations of the data, the strange secondary peaks are seen again in this trajectory, creating a peak in the positive x (thrust) and negative y (lift) direction. In Figure 3-13 the peaks are seen at around the $t = 0.5s$ mark, and in in Figure 3-14 the last two force vectors point in the positive x and negative y direction. As with the other trajectories, the wake produced by Trajectory 5 was studied using the dye visualization setup explained in Section 2.3.

3.3.3 Dye Visualisation

For the dye visualization experiment for Trajectory 4, holes in the custom wing allow the dye to flow from the leading and trailing edge, red from the leading edge and blue from the trailing edge. This trajectory was filmed from both cameras as explained in Section 2.3, capturing features from both the beginning and end of the trajectory. Additionally, the dye visualization was performed at a slower speed. This does produce the same flow, as explained in Appendix A. The features from the beginning and middle of the trajectory were best captured by Camera A, and the wake structures at the end of the stroke were best captured by Camera B; however the images have

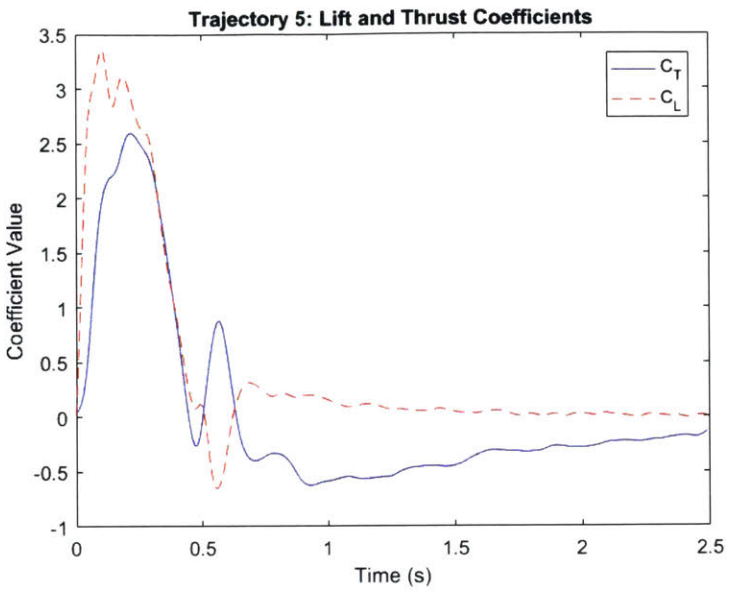

Figure 3-13: Force results from Trajectory 5. Presented here as C_L and C_T, as described in Section 2.1

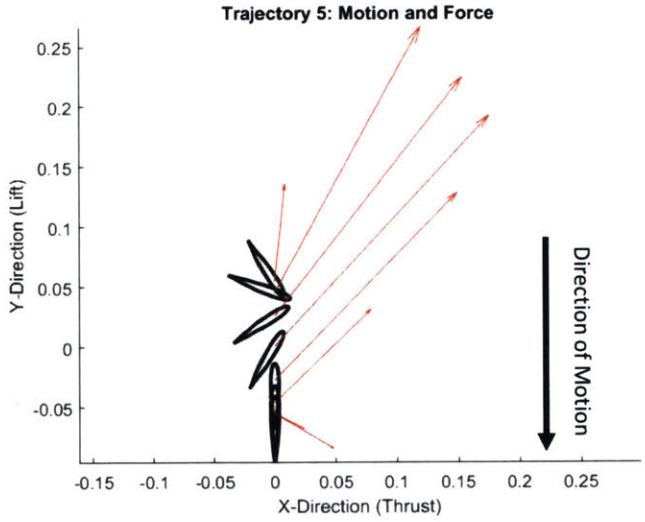

Figure 3-14: Visualization of the forces produced by Trajectory 5.

been rotated/flipped for the diagram.

Figure 3-15 shows the results of the visualization; the beginning of the stroke is shown in Figure 3-15(a) and shows a trailing edge vortex (in the blue dye) fully formed as a leading edge vortex (in the red dye) forms. Similar to Trajectory 4, in Figure 3-15(b) the red LEV remains attached while the blue TEV gets left behind as the foil pitches faster than it heaves. What differs here is that as the "quick turn"

happens, as shown in Figure 3-15(c), the blue TEV completely detaches, and the LEV and TEV form a doublet-like structure. in Figure 3-15(d), just after the quick turn, an additional doublet like structure forms at the trailing edge of the foil, with this doublet slowly merging together. In Figure 3-15(e), just at the end of the trajectory, the merged doublet remains close to the foil, while the LEV/TEV doublet is relatively far away. Due to the suction forces, the merged doublet creates the smaller peak in the positive X, negative Y Direction seen in the force data. After the second peak(s), a smaller, more consistent force appears, and is the result of the small red vortex seen in Figure 3-15(f). Like the other trajectories, the unexplained forces seen in the force data are due to interactions between the foil and its own wake structures.

3.4 Trajectory 6.1

3.4.1 Kinematics

This trajectory is one of three (6.1, 6.2, and 6.3) that explored more or less the same concept. To maximize positive lift force, the foil remains at $\theta = 0$, and does a quick-turn to $\theta = +\pi/2$, but does so smoothly. The three trajectories differ in the duration of the quick turn, where 6.1 is the quickest (turn duration of 0.2s), followed by 6.2 (turn duration of 0.27s), and 6.3 has the longest turn (turn duration of 0.35s) from $\theta = 0$ to $\theta = +\pi/2$. Figure 3-16 shows a more detailed description of the trajectory, including heave and pitch positions, velocities, and accelerations as functions of time. Figure 3-17 shows a visualization of the trajectory.

3.4.2 Force Results

The force data produced by Trajectory 6.1 are shown in Figure 3-18, presented in non-dimensional form described in Section 2.1, and a more visual representation of the force data is shown in Figure 3-19. The desired effect, a large lift force, was recorded with very small thrust forces, caused by the turn. Additionally, the strange combination of positive X (thrust), and negative Y (lift) peaks occur here as the wing

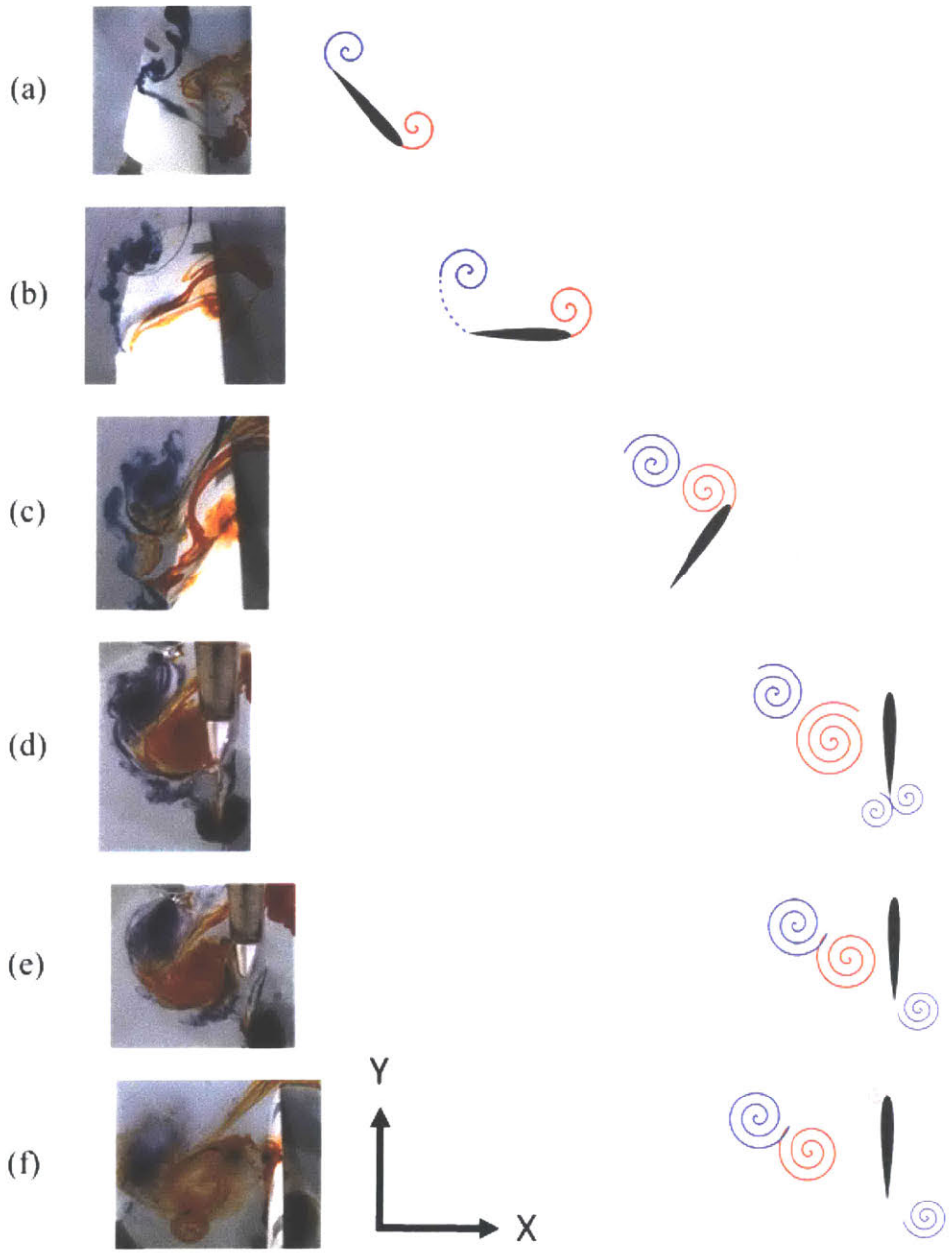

Figure 3-15: Dye visualization images and diagram of Trajectory 5.

comes to a stop. Like the other trajectories tested before this one, it is most likely caused by the interactions of the wing and its own vortical wake structures.

3.4.3 Dye Visualisation

As explained in Section 2.3, holes in the custom wing allow the dye to flow from the leading and trailing edge, red from the leading edge and blue from the trailing

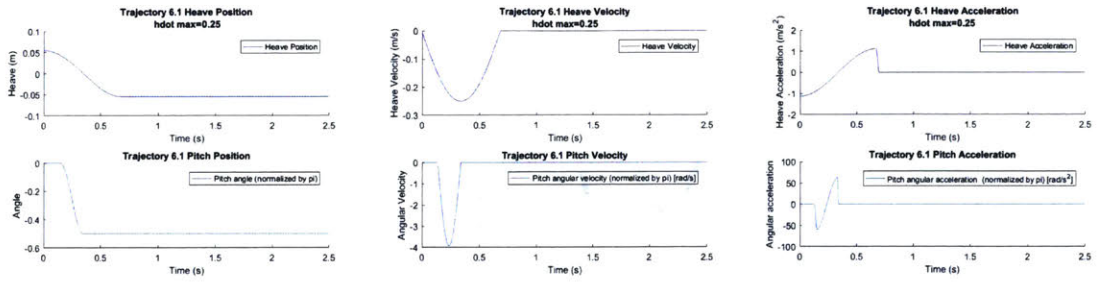

(a) (b) (c)

Figure 3-16: Kinematics of the foil's motion during Trajectory 6.1. Heave and pitch position are shown in (a), heave and pitch velocity are shown in (b), and heave and pitch acceleration are shown in (c).

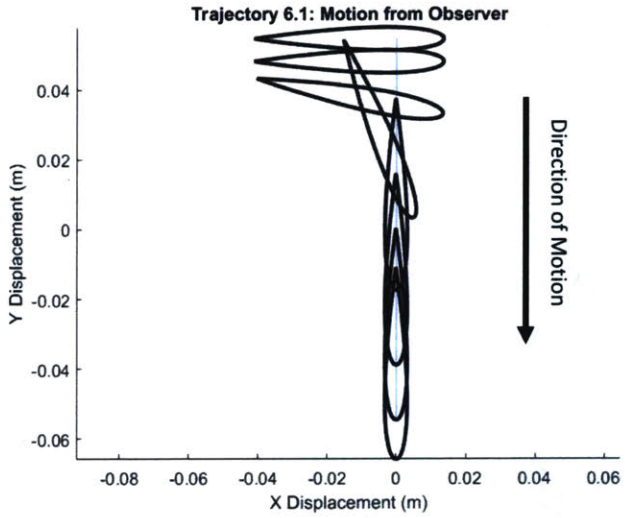

Figure 3-17: Visualization of the foil's motion during Trajectory 6.1.

edge.This trajectory was filmed from both cameras as explained in Section 2.3, capturing features from both the beginning and end of the trajectory. The features from the beginning and middle of the trajectory were best captured by Camera A, and the wake structures at the end of the stroke were best captured by Camera B, but the images from each camera have been rotated/flipped for the diagram for clarity.

Figure 3-20 shows the results of the visualization; the beginning of the stroke is shown in Figure 3-20(a) which shows the simultaneous formation of leading (in red) and trailing edge (in blue) vortices, as the foil moves downward in heave without pitching. Later in the stroke, as shown in Figure 3-20(b), about halfway through the 'quick turn', the foil brings the leading edge vortex with it as it goes through the

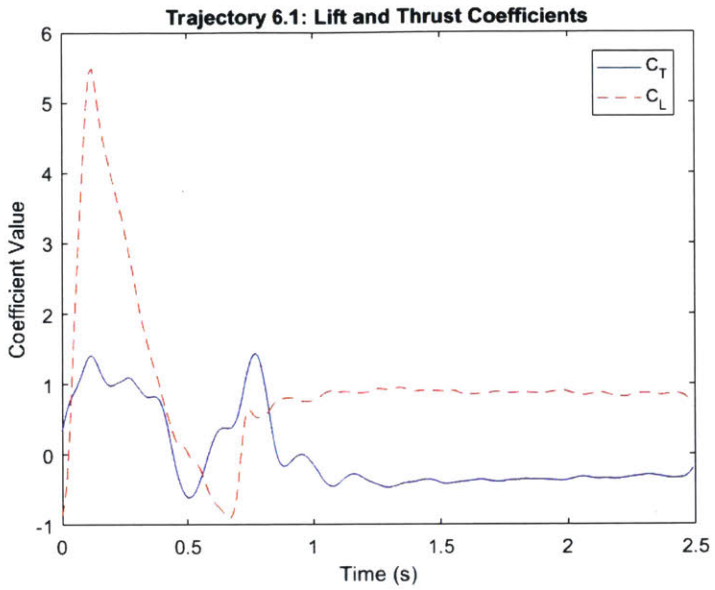

Figure 3-18: Force results from Trajectory 6.1. Presented here as C_L and C_T, as described in Section 2.1

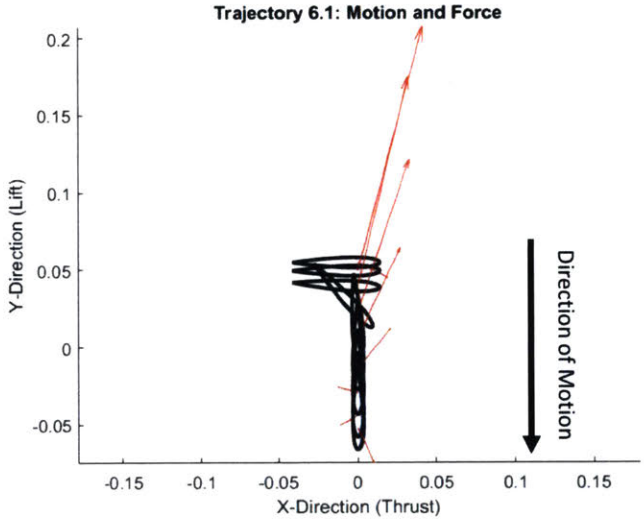

Figure 3-19: Visualization of the forces produced by Trajectory 6.1.

pitching motion, and the TEV begins to separate. Figure 3-20(c) shows the part of the stroke just as the foil comes to a stop, where the LEV is pulling blue dye into it, and this suction creates a force in the negative y (lift) and positive x (thrust) direction (following the coordinates on the figure), just as is seen in the force results above. In a similar manner to Trajectory 1.1, explained in Section 3.1, after the end of the stroke, a small, blue vortex appears; its suction creates the small amount of

positive y (lift) and negative x (thrust) force seen in the force results after around $t = 1s$. Like all the other experiments, the interactions between the foil and its wake structures produce the additional peaks seen in the force data.

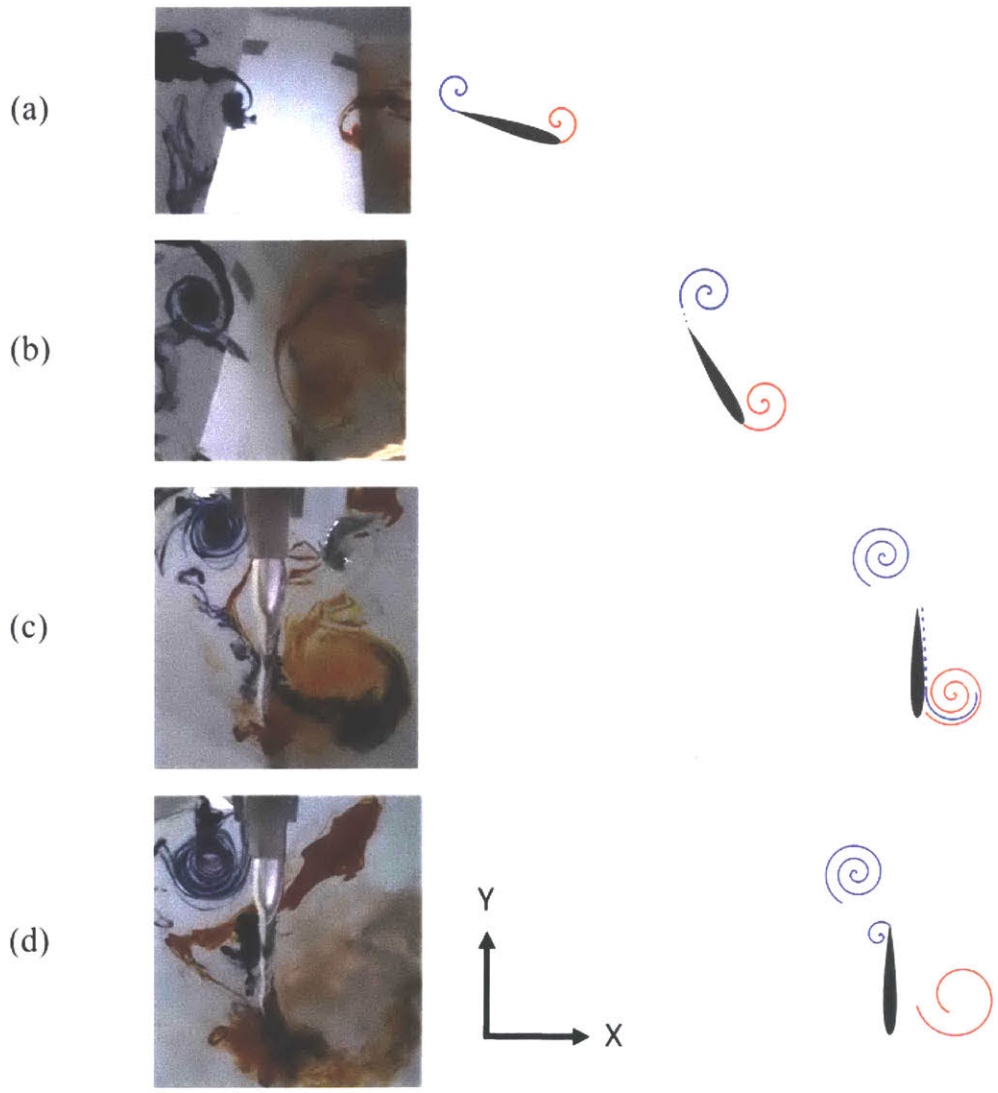

Figure 3-20: Dye visualization images from Trajectory 6.1.

3.5 Trajectory 6.2

3.5.1 Kinematics

Trajectory 6.2 is the second of three trajectories that explored the duration of a quick turn in pitch from $\theta = 0$ to $\theta = -\pi/2$. Here, the quick turn is slightly longer than the

turn in Trajectory 6.1 (Trajectory 6.1 has a turn duration of 0.2s while Trajectory 6.2 has a turn duration of 0.27s), but is still smooth. The more detailed kinematics can be seen in Figure 3-21, including heave and pitch positions, velocities, and accelerations as functions of time, and Figure 3-22 shows a visual representation of the trajectory.

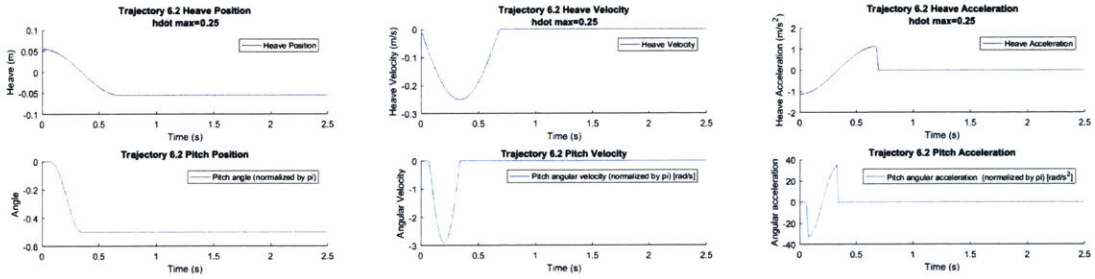

(a) (b) (c)

Figure 3-21: Kinematics of the foil's motion during Trajectory 6.2. Heave and pitch position are shown in (a), heave and pitch velocity are shown in (b), and heave and pitch acceleration are shown in (c).

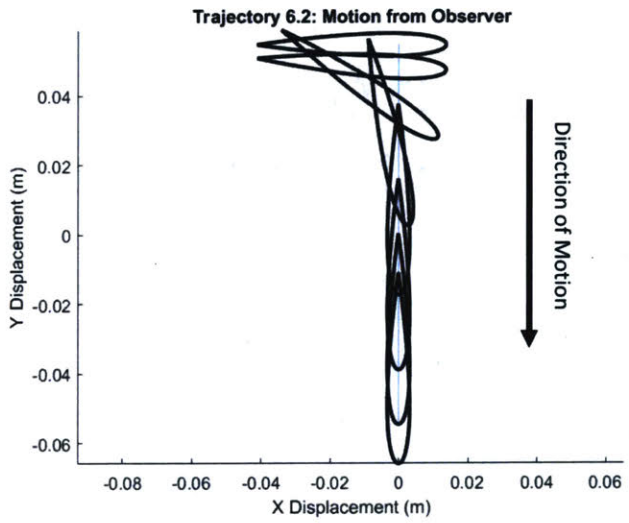

Figure 3-22: Visualization of the foil's motion during Trajectory 6.2.

3.5.2 Force Results

The force results from Trajectory 6.2 are shown in Figure 3-23, and more visually intuitive representation of these data are shown in Figure 3-24. As one would expect, the results for Trajectories 6.1 and 6.2 are very similar. The foil produces a large

lift peak with positive thrust force, and as the trajectory reaches its end (around 0.7s), the peak in positive X-direction (thrust) and negative Y-direction (lift) force appears once again. As with the other instances in which this peak appeared, the dye visualization showed that this is a result of the foil interacting with its own wake structures.

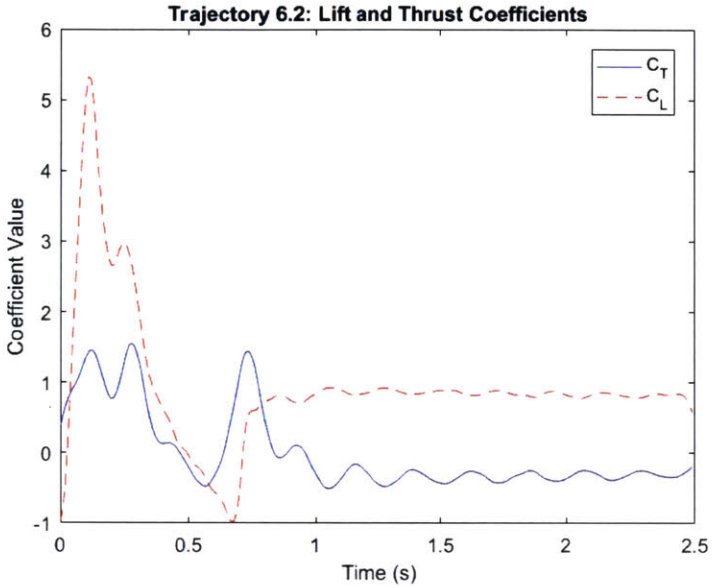

Figure 3-23: Force results from Trajectory 6.2. Presented here as C_L and C_T, as described in Section 2.1

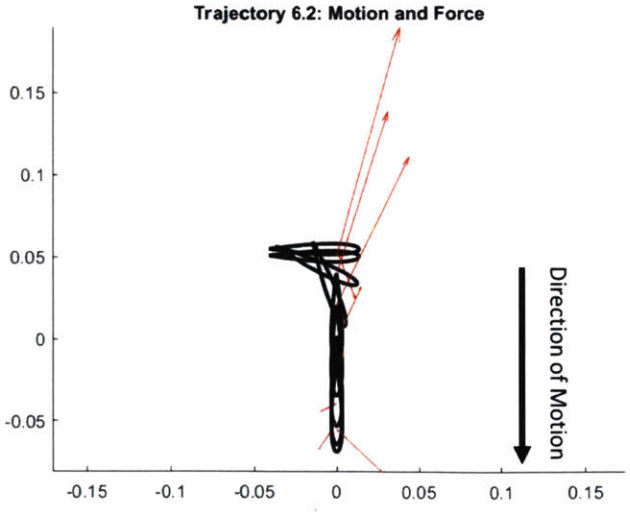

Figure 3-24: Visualization of the forces produced by Trajectory 6.2.

As explained in Section 2.3, holes in the custom wing allow the dye to flow from the leading and trailing edge, red from the leading edge and blue from the trailing edge.This trajectory was filmed from both cameras as explained in Section 2.3, capturing features from both the beginning and end of the trajectory. The features from the beginning and middle of the trajectory were best captured by Camera A, and the wake structures at the end of the stroke were best captured by Camera B (in a different trial), but the images from each camera have been rotated/flipped for the diagram for clarity.

Unsurprisingly, the dye visualization results resemble those from Trajectory 6.1. Figure 3-25 shows the results of the visualization; the beginning of the stroke is shown in Figure 3-25(a) which shows the simultaneous formation of leading (in red) and trailing edge (in blue) vortices, as the foil moves downward in heave without pitching. Later in the stroke, as shown in Figure 3-25(b), about halfway through the 'quick turn', the foil brings the leading edge vortex with it as it goes through the pitching motion, and the TEV begins to separate. Figure 3-25(c) shows the part of the stroke just as the foil comes to a stop, where the LEV is pulling blue dye into it, and this suction creates a force in the negative y (lift) and positive x (thrust) direction (following the coordinates on the figure), just as is seen in the force results above. In a similar manner to Trajectory 1.1, explained in Section 3.1, after the end of the stroke, a small, blue vortex appears; its suction creates the small amount of positive y (lift) and negative x (thrust) force seen in the force results after around $t = 1s$. Like all the other experiments, the interactions between the foil and its wake structures produce the additional peaks seen in the force data.

3.6 Trajectory 6.3

3.6.1 Kinematics

Trajectory 6.3 is the last of the three trajectories that explored the duration of a quick turn in pitch from $\theta = 0$ to $\theta = -\pi/2$ during the heave motion. Here, the

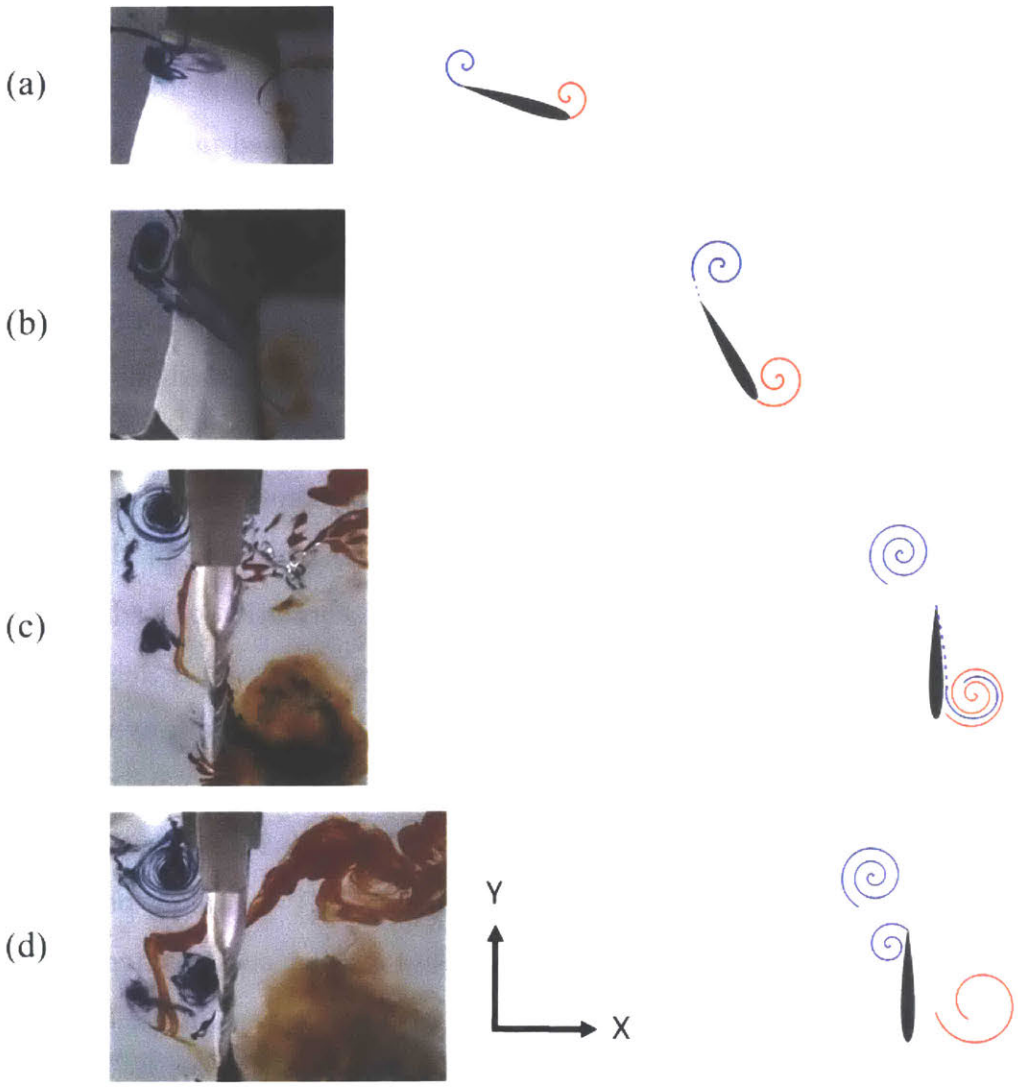

Figure 3-25: Dye visualization images from Trajectory 6.2.

quick turn is the longest of the three (Trajectory 6.1 has a turn duration of 0.2s, Trajectory 6.2 has a turn duration of 0.27s, but Trajectory 6.3 has a turn duration of 0.35s), but is still smooth. The more detailed kinematics can be seen in Figure 3-26, including heave and pitch positions, velocities, and accelerations as functions of time, and Figure 3-27 shows a visual representation of the trajectory. As seen in the figures, the foil spends almost no time moving in heave without pitching, making it resemble Trajectory 1 slightly.

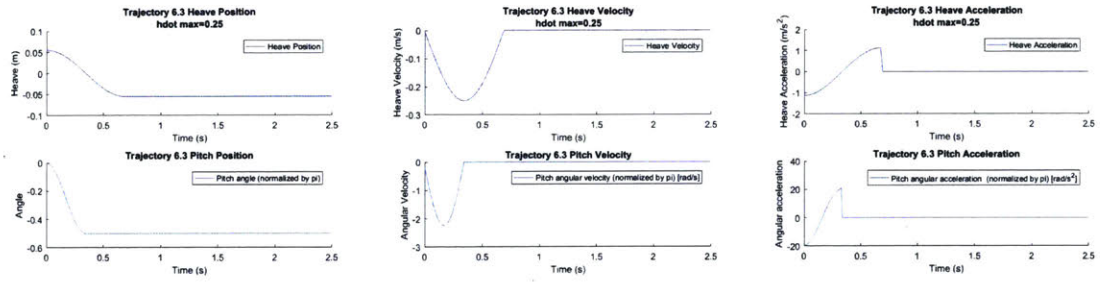

(a) (b) (c)

Figure 3-26: Kinematics of the foil's motion during Trajectory 6.3. Heave and pitch positions are shown in (a), heave and pitch velocities are shown in (b), and heave and pitch accelerations are shown in (c).

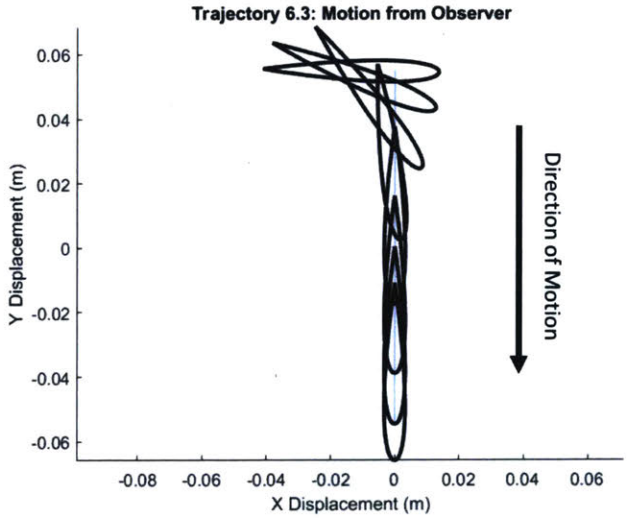

Figure 3-27: Visualization of the foil's motion during Trajectory 6.3.

3.6.2 Force Results

The force results from Trajectory 6.3 are shown in Figure 3-28, and more visually intuitive representation of these data are shown in Figure 3-29. As one would expect, the results for Trajectories 6.1, 6.2, and 6.3 are all very similar to one another. The foil produces a large lift peak with positive thrust force, and as the trajectory reaches its end (around 0.7s), the peak in positive X-direction (thrust) and negative Y-direction (lift) force appears once again. As with the other instances in which this peak appeared, the dye visualization showed that this is a result of the foil interacting with its own wake structures.

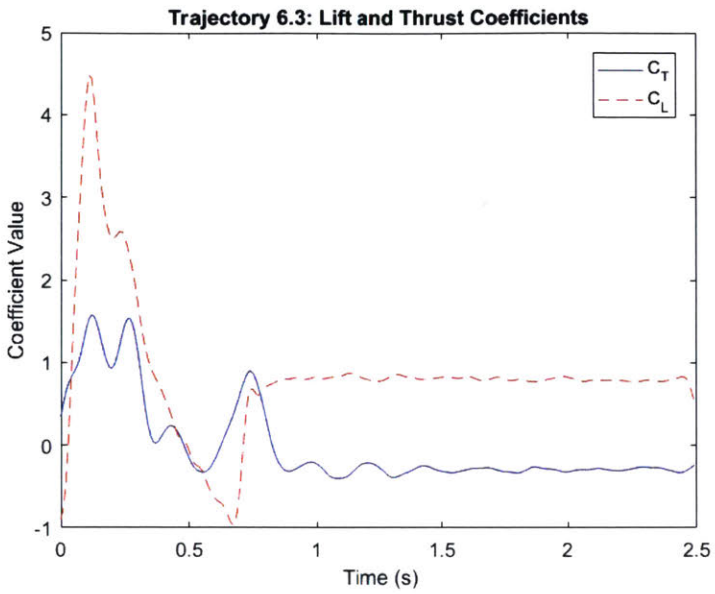

Figure 3-28: Force results from Trajectory 6.3 Presented here as C_L and C_T, as described in Section 2.1

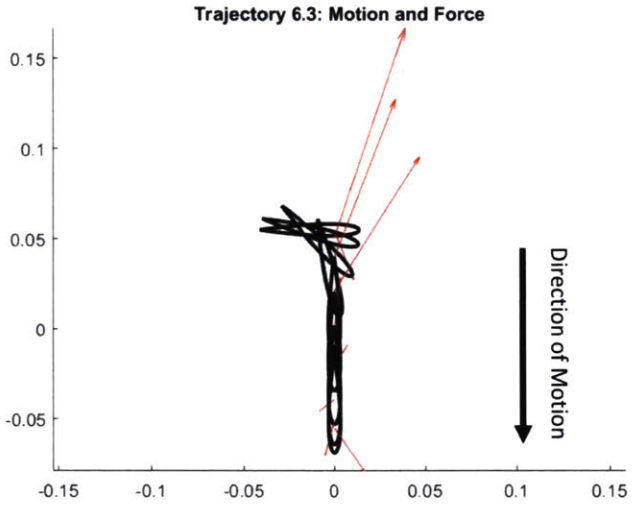

Figure 3-29: Visualization of the forces produced by Trajectory 6.3.

3.6.3 Dye Visualisation

As explained in Section 2.3, holes in the custom wing allow the dye to flow from the leading and trailing edge, red from the leading edge and blue from the trailing edge.This trajectory was filmed from both cameras as explained in Section 2.3, capturing features from both the beginning and end of the trajectory. The features from

the beginning and middle of the trajectory were best captured by Camera A, and the wake structures at the end of the stroke were best captured by Camera B, but the images from each camera have been rotated/flipped for the diagram for clarity.

Unsurprisingly, the dye visualization results resemble those from Trajectory 6.1 and 6.2. Figure 3-30 shows the results of the visualization; the beginning of the stroke is shown in Figure 3-30(a) which shows the simultaneous formation of leading (in red) and trailing edge (in blue) vortices, just as the foil begins its motion and before any significant pitch transition happens. Later in the stroke, as shown in Figure 3-30(b), about halfway through the 'quick turn', the foil brings the leading edge vortex with it as it goes through the pitching motion, and the TEV begins to separate. Figure 3-30(c) shows the part of the stroke just as the foil comes to a stop, where the LEV is pulling blue dye into it, and this suction creates a force in the negative y (lift) and positive x (thrust) direction (following the coordinates on the figure), just as is seen in the force results above. In a similar manner to Trajectory 1.1, explained in Section 3.1, after the end of the stroke, a small, blue vortex appears; its suction creates the small amount of positive y (lift) and negative x (thrust) force seen in the force results after around $t = 1s$. Like all the other experiments, the interactions between the foil and its wake structures produce the additional peaks seen in the force data.

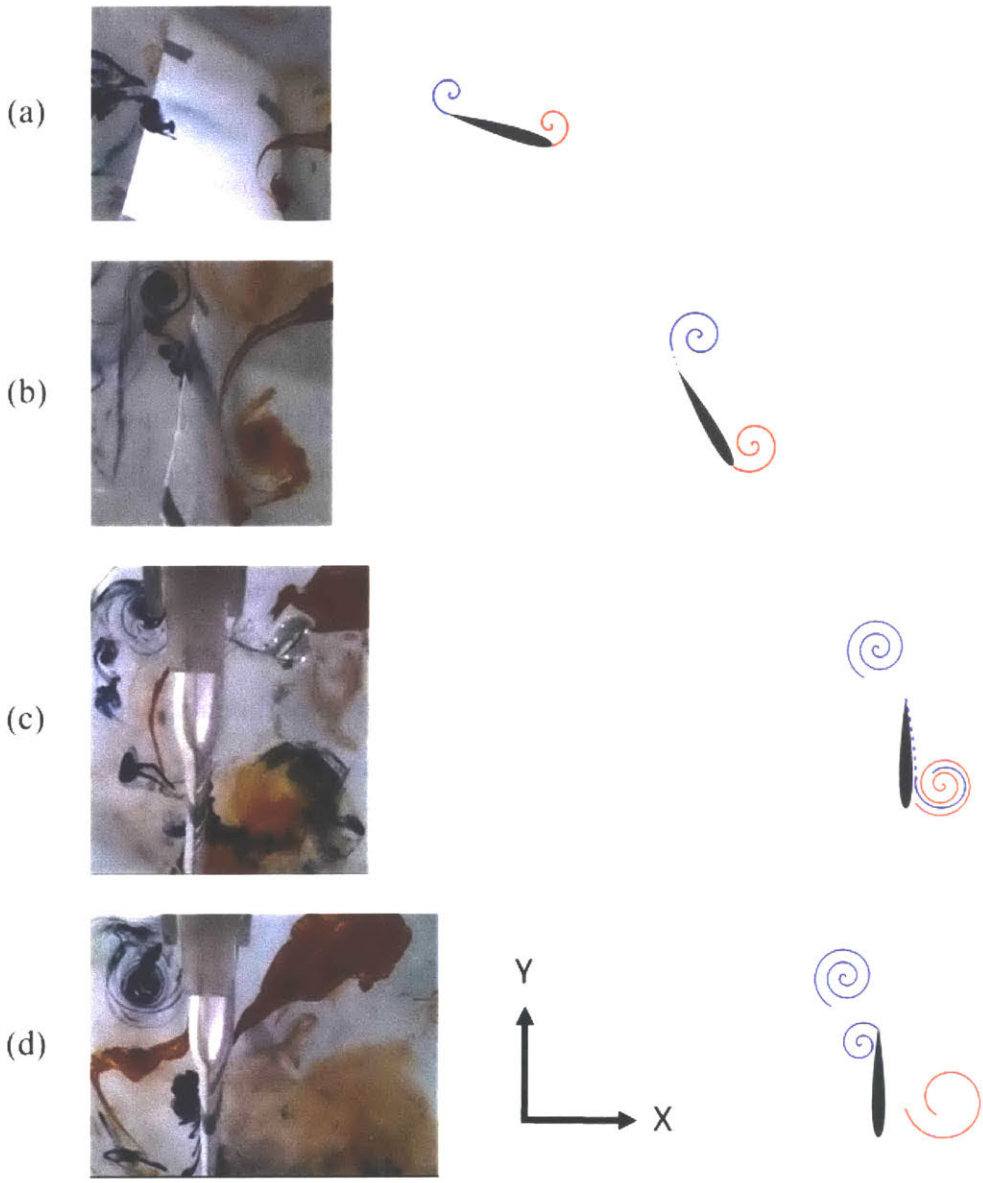

Figure 3-30: Dye visualization images from Trajectory 6.3.

Chapter 4

Conclusion

Inspired by the natural world of underwater animals, transient motions of flapping foils in calm water were investigated, continuing the work begun in (Triantafyllou et al., 2003). The foils were moved along prescribed motions of heave and pitch, and the resulting forces were recorded. Using creative combinations of heave and pitch motions of the wing, large, transient forces were produced. Additionally, the effect of timing was explored, and found that the duration of a "quick turn" has little effect on the overall shape of the force profile, but has a small effect on the magnitude of the forces produced. The most important and interesting results of this work came from the dye visualization experiments. A custom designed wing moved along the prescribed heave and pitch motions, and the resulting wake and wake structures were recorded using GoPro cameras. In all of the foil motions, significant interactions between the foil and the wake structures were noticed, and explained mysterious peaks seen in the force results. These interactions seem to make producing a "pure" lift and/or thrust force extremely difficult, as the foil cannot escape its own wake. Overall, the trajectories tested were an extremely promising step in the investigation of transient motions of flapping foils and bode well for the future of underwater vehicles. As underwater swimmers do, the flapping foil could be used as an actuator to produce these forces to control an underwater vehicle's position, orientation, or heading.

Future work would include further elucidating the interactions between the foil

and the wake structures it produces during the stroke. This could be done with additional dye visualization experiments (from different viewpoints, perhaps), or with more sophisticated flow visualization techniques, such as Particle Image Velocimetry (PIV). Additionally, numerical methods could be used to simulate these types of strokes for the force result and/or for visualization. This is part of the larger goal of optimizing the heave and pitch motions to either mitigate or take advantage of these wake structures and the resulting interactions. A parallel option for the future of this work is investigating the engineering challenges and benefits of this type of actuator. If a vehicle utilizes these transient strokes onboard, the forces produced by the wing(s) would produce motion of the vehicle, and with it, the wing itself. This would significantly change the interactions between the wing and the wake structures (if there are any interactions at all), and is also more representative of the ultimate goal: changing the way underwater vehicles move and maneuver through the water.

Appendix A

Dye Visualization Speed Comparison

In Trajectories 4 and 5, the dye visualization experiments were done at a different, slower speed than the force experiments. This was to prevent bending and/or structural damage in the dye visualization custom wing and for clarity of the visualization results. To ensure that the trajectory at two different speeds would produce the same flow, we compare the velocity in heave to the velocity produced by changes in pitch. To get these velocities, we start with the heave and pitch positions.

The heave motions follow this general form:

$$h(t) = ccos(\omega_h t)$$

where c is the chord length of the foil, and $\omega_h = \frac{\dot{h}_{max}}{c}$. $\dot{h}_{max}$ describes the 'speed' of the stroke, and appears in Section 2.1 in the calculaion of non-dimensional force values, referred to as C_L and C_T throughout the thesis. The pitch motions follow the form:

$$\theta(t) = \theta_0 cos(\omega_\theta t)$$

where θ_0 is the starting value of the pitch motion (and varies between the trajectories), and ω_θ determines the 'speed' of the pitch motion. In Trajetory 4, $\omega_\theta = \frac{3}{4}\omega_h$, and thus creates a longer pitch motion, which causes the period of pure pitch at the end of the trajectory, seen in Section 3.2. In Trajectory 5, $\omega_\theta = 2\omega_h$, and is followed

by the quick turn, explained in Section 3.3.

Now, to compare velocities. To compare heave velocity to pitch, we must multiply the angular velocity by a length measurement , so the chord length c is used.

For the heave velocity,

$$V_h = c\omega_h(-sin(\omega_h t))$$

And for the velocity from pitch,

$$V_p = -c\theta_0\omega_\theta sin(\omega_\theta t)$$

To remove the time-varying component of these velocities, we will compare the ampitudes of the sinusoids. So,

$$\frac{V_h}{V_p} = \frac{c\omega_h}{c\theta_0\omega_\theta} = \frac{\omega_h}{\theta_0\omega_\theta}$$

For Trajectory 4, $\omega_\theta = \frac{3}{4}\omega_h$, which makes,

$$\frac{V_h}{V_p} = \frac{4\omega_h}{\theta_0(3\omega_h)} = \frac{4}{3\theta_0}$$

This result is only dependent on the starting value of the pitch, which remains the same between the force experiment the dye visualization experiment for Trajectory 4.

For Trajectory 5, $\omega_\theta = 2\omega_h$, so a similar result is found:

$$\frac{V_h}{V_p} = \frac{\omega_h}{\theta_0(2\omega_h)} = \frac{1}{2\theta_0}$$

This result also only depends on the starting value of pitch, which remains the same between the force experiment and the dye visualization experiment for Trajectory 5.

Overall, Trajectories 4 and 5 produce the same wake characteristcs, regardless of speed.

Bibliography

P. R. Bandyopadhyay. Guest editorial: Biology-inspired science and technology for autonomous underwater vehicles. *IEEE Journal of Oceanic Engineering*, 29(3): 542–546, July 2004. ISSN 0364-9059. doi: 10.1109/JOE.2004.833099.

P. R. Bandyopadhyay. Trends in biorobotic autonomous undersea vehicles. *IEEE Journal of Oceanic Engineering*, 30(1):109–139, Jan 2005. ISSN 0364-9059. doi: 10.1109/JOE.2005.843748.

P. R. Bandyopadhyay, J. M. Castano, J. Q. Rice, R. B. Philips, W. H. Nedderman, and W. K. Macy. Low-Speed Maneuvering Hydrodynamics of Fish and Small Underwater Vehicles. *Journal of Fluids Engineering*, 119(1):136–144, 03 1997. ISSN 0098-2202. doi: 10.1115/1.2819099. URL `https://doi.org/10.1115/1.2819099`.

F.E. Fish and G.V. Lauder. Passive and active flow control by swimming fishes and mammals. *Annual Review of Fluid Mechanics*, 38(1):193–224, 2006. doi: 10.1146/annurev.fluid.38.050304.092201. URL `https://doi.org/10.1146/annurev.fluid.38.050304.092201`.

FormLabs. Formlabs form 2, November 2018. URL `https://formlabs.com/3d-printers/form-2/`.

N. Kato. Control performance in the horizontal plane of a fish robot with mechanical pectoral fins. *IEEE Journal of Oceanic Engineering*, 25(1):121–129, Jan 2000. ISSN 0364-9059. doi: 10.1109/48.820744.

Naomi Kato. Locomotion by mechanical pectoral fins. *Journal of Marine Science and Technology*, 3(3):113–121, Sep 1998. ISSN 1437-8213. doi: 10.1007/BF02492918. URL `https://doi.org/10.1007/BF02492918`.

G. V. Lauder and E. G. Drucker. Morphology and experimental hydrodynamics of fish fin control surfaces. *IEEE Journal of Oceanic Engineering*, 29(3):556–571, July 2004. ISSN 0364-9059. doi: 10.1109/JOE.2004.833219.

George V. Lauder and Peter G. A. Madden. Learning from fish: Kinematics and experimental hydrodynamics for roboticists. *International Journal of Automation and Computing*, 3(4):325–335, Oct 2006. ISSN 1751-8520. doi: 10.1007/s11633-006-0325-0. URL `https://doi.org/10.1007/s11633-006-0325-0`.

George V Lauder, Peter G A Madden, Rajat Mittal, Haibo Dong, and Meliha Bozkurttas. Locomotion with flexible propulsors: I. experimental analysis of pectoral fin swimming in sunfish. *Bioinspiration & Biomimetics*, 1(4):S25–S34, dec 2006. doi: 10.1088/1748-3182/1/4/s04. URL `https://doi.org/10.1088%2F1748-3182%2F1%2F4%2Fs04`.

George V. Lauder, Erik J. Anderson, James Tangorra, and Peter G. A. Madden. Fish biorobotics: kinematics and hydrodynamics of self-propulsion. *Journal of Experimental Biology*, 210(16):2767–2780, 2007. ISSN 0022-0949. doi: 10.1242/jeb.000265. URL `https://jeb.biologists.org/content/210/16/2767`.

S. Licht, F. Hover, and M. S. Triantafyllou. Design of a flapping foil underwater vehicle. In *Proceedings of the 2004 International Symposium on Underwater Technology (IEEE Cat. No.04EX869)*, pages 311–316, April 2004. doi: 10.1109/UT.2004.1405590.

MJ Lighthill. Hydromechanics of aquatic animal propulsion. *Annual review of fluid mechanics*, 1(1):413–446, 1969.

D.A. Read, F.S. Hover, and M.S. Triantafyllou. Forces on oscillating foils for propulsion and maneuvering. *Journal of Fluids and Structures*, 17(1):163 – 183, 2003. ISSN 0889-9746. doi: https://doi.org/10.1016/S0889-9746(02)00115-9. URL `http://www.sciencedirect.com/science/article/pii/S0889974602001159`.

M. S. Triantafyllou. Personal communication, 2017.

M. S. Triantafyllou, F. Hover, and S. Licht. The mechanics of force production in flapping foils under steady-state and transient motion conditions. Testing Tank Facility Report 031903, Massachusetts Institute of Technology, Department of Ocean Engineering, Cambridge, Massachusetts, March 2003.

MS Triantafyllou, DS Barrett, K Streitlien, and JM Anderson. Flapping foils of high propulsive efficiency. *Journal of Fluid Mechanics*, 1996.